

# Preliminary geology of the Shrimpton Creek area (NTS 092H/15E, 16W) Southern Nicola Arc Project

Mitchell G. Mihalynuk<sup>1, a</sup>, Larry J. Diakow<sup>1</sup>, James M. Logan<sup>2</sup>, and Richard M. Friedman<sup>3</sup>

<sup>1</sup> British Columbia Geological Survey, Ministry of Energy and Mines, Victoria, BC, V8W 9N3

<sup>2</sup> JLoGeologic, Victoria, BC, V8L 5Z9

<sup>3</sup> Pacific Centre for Geochemical and Isotopic Research, University of British Columbia, Vancouver, BC, V6T 1Z4

<sup>a</sup> corresponding author: Mitch.Mihalynuk@gov.bc.ca

Recommended citation: Mihalynuk, M.G., Diakow, L.J., Logan, J.M., and Friedman, R.M., 2015. Preliminary geology of the Shrimpton Creek area (NTS 092H/15E, 16W) Southern Nicola Arc Project. In: Geological Fieldwork 2014, British Columbia Ministry of Energy and Mines, British Columbia Geological Survey Paper 2015-1, pp. 129-163.

---

## Abstract

Geological maps and analytical results of the Southern Nicola Arc Project (SNAP) change the way that we view the evolution of southern Quesnel terrane. Nicola arc rocks host the Copper Mountain mine to the south and the Highland Valley and Afton mines to the north of the SNAP study area. Nicola Arc has been classically thought of as Late Triassic, felsic in the west, and relatively unaffected by contractional deformation. Our work indicates that magmatism is older (~238 Ma) than previously known and that the oldest dated Nicola Group rocks are felsic units in the central part of the arc. Felsic volcanism is not restricted to the classical 'Western belt' where it is now well dated at 224 to 225 Ma. Here we report on the Shrimpton area (NTS 092H/15E, 16W) where the oldest rocks are inferred to be turbiditic strata of the Eastern siliciclastic succession, which underlie the eastern map boundary. Near the western map boundary, the youngest dated Nicola Group rocks are volcanic sandstones. Zircons from the basal beds and a crosscutting dike limit deposition to between ~208 and ~201 Ma. These strata are capped by andesitic volcanic rocks of the 'Tillery unit'. Between the Eastern succession and the Tillery unit, we mapped volcanic and sedimentary units that can be traced for ten km or more. Many of these units have been assigned to one of three successions: 'Paradise', 'Shrimpton' and 'Harmon'. Thick volcanic conglomerates comprise the 'Paradise succession'. 'Shrimpton succession' includes finer clastic rocks, but also more arc-proximal, distinctive, apatite- biotite- and quartz-phyric tuffaceous rocks of the 'Zig unit'. These contain probable syngenetic Cu-Ag mineralization dated at ~210 Ma. Above the Shrimpton succession is the fossiliferous 'Hendriks limestone' of probable Norian age. It is incised by a regional unconformity upon which the Harmon succession was deposited, starting with the polymictic 'Shea conglomerate'. A return to arc construction is recorded by the Voght unit: coarse bladed feldspar porphyry flows that are intercalated with volcanic sandstone, mostly deposited above beds containing the >208 Ma detrital zircons. Overlying the Nicola Group is the 'Bates unit', an enigmatic chert pebble conglomerate with no known local source. Andesite to rhyolite of the Spences Bridge Group (~103-104 Ma) probably overly Bates conglomerate, loosely constraining its age to between 201 Ma and 104 Ma. Evidence for contractional deformation that regionally affects strata as young as Middle Jurassic (~170 Ma) is widespread. However, older deformation is also inferred from regional unconformities within the Nicola Group, and north-northeast synkinematic fabrics in the Late Triassic Allison pluton. Nicola arc rocks and their prolific porphyry deposits have been the primary target for mineral exploration in the area, but significant mineralization is also present in younger magmatic units, like the Osprey batholith (155-165 Ma) and the Otter intrusions (~53 Ma) that cut Nicola arc rocks. Examples are gold veins at the Siwash mine and, 8 km to the south, intense clay alteration around quartz stockworks containing pyrite-sphalerite-galena-chalcocopyrite at the Snowstorm prospect. Pyrite-sphalerite-galena-chalcocopyrite mineralization mapped 6 km east of the Snowstorm is not recorded in MINFILE. If related, it gives significant dimension to the magmato-hydrothermal system.

**Keywords:** porphyry copper gold, volcanogenic massive sulphide, gold vein, Miner Mountain, Siwash mine, Par prospect, Snowstorm prospect, Princeton, Merritt, Nicola Group, Spences Bridge Group, Princeton Group, Chilcotin Group, paleogeography

---

## 1. Introduction

Fieldwork in the prolifically mineralized southern Nicola belt (Figs. 1, 2) extended over about six months split between the summers of 2013 and 2014. New exposures and access arising from extensive clear-cut timber harvesting during salvage operations following the Mountain Pine Beetle infestation significantly benefit our geological mapping program. Such access was mostly lacking during creation of the benchmark geological work in the area at least three decades ago (Schau, 1968; Christopher, 1973; Lefebure, 1976; Preto, 1979; Monger, 1989). Herein we present new map, stratigraphic, geochronologic, structural, and mineral deposit data collected to better understand the evolution of the Nicola arc and the

major controls of mineralization. Our aim is to illuminate further exploration opportunities in a mining camp that, for 50 years, has contributed significantly to the wealth of British Columbians through copper and gold production.

## 2. Geography and Geological setting

On the dissected plateau between the Coast-Cascades ranges and orographic desert of the Interior Plateau, exposures of Nicola arc rocks are sparse. Only along steep valleys and glacially scoured ridges are continuous exposures found. However, extensive networks of logging roads and two highways provide excellent access to almost all parts of the map area. Away from roads, foot travel is easy through typically dry,

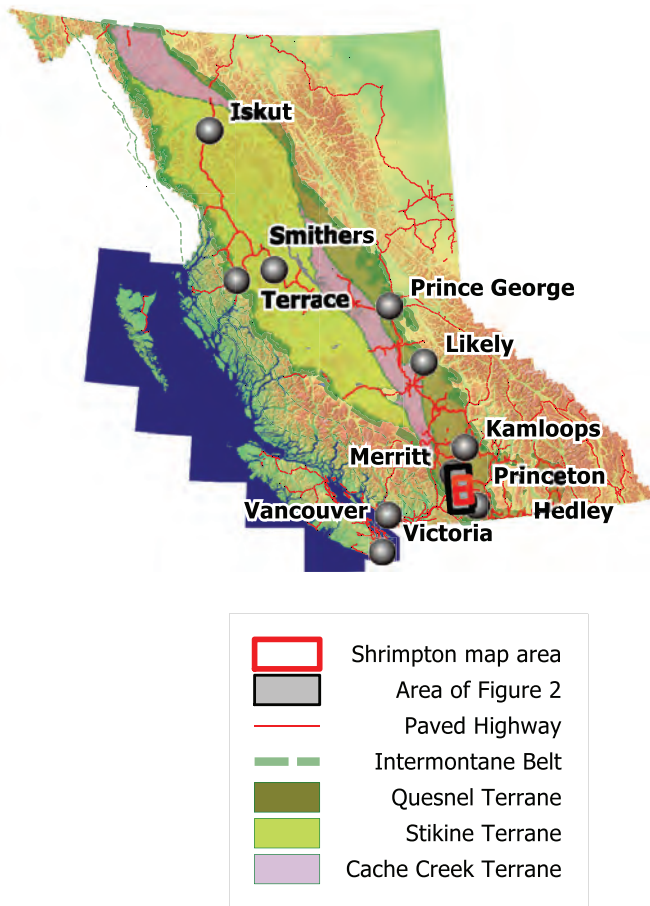


**Fig. 1.** Physiographic and tectonic setting of the Southern Nicola Arc Project (SNAP) study area between Princeton and Merritt.

open pine forests, and grassland.

Tributaries of three south-flowing creeks drain the southern map area. From west to east they are: Otter, Shrimpton (flows into Summers Creek via Missezula Lake), and Siwash (Fig. 3). Most of the northern map area is within the Quilchena Creek drainage, which eventually flows north into Nicola Lake. An exception is the northwest map area, which drains into Voght Creek, and eventually, the Coldwater River at Kingsvale (Fig. 2).

Nicola arc is constructed on basement rocks of a composite island arc belonging to the Quesnel terrane that contains fossils as old as Late Silurian (Read and Okulitch, 1977). The basement arc probably began life at the distal margin of western North America in the Devonian (Monger et al., 1972; Monger, 1977; Mihalynuk et al., 1994; Ferri, 1997). A back-arc basin apparently formed as this arc was rifted from its continental margin homeland (Harms, 1986; see discussions in Ferri, 1997; Mihalynuk et al., 1999; and citations therein). As the back-arc basin grew to oceanic proportions, the relicts of which are known by various names, most commonly 'Slide Mountain' in the south and 'Angayucham' in the north, Quesnellia became isolated from North America permitting colonization of endemic organisms, the remains of which are

not seen in adjacent parts of cratonic North America (Ross and Ross, 1983 and 1985; Belasky et al., 2002). The Slide Mountain basin began to close in the Permian (Struik and Orchard, 1985), probably initiated as a consequence of plate tectonic readjustments following the final closing of the Rheic Ocean (Nance et al., 2012) on the far side of North America. Quesnel and Stikine terranes started to be swept up against North America in the Late Triassic, which was accelerating westward with fragmentation of Pangea and growth of the new Atlantic Ocean. Both terranes were repatriated with the North American continental margin by the Early Jurassic (~185 Ma, Nixon et al., 1993); but final buckling and entrapment of exotic oceanic rocks of the Cache Creek between Quesnel and Stikine terranes was not completed until the Middle Jurassic (Ricketts et al., 1992; Monger and Ross, 1971; Mihalynuk et al., 1994; ~172 Ma, Mihalynuk et al., 2004). After the Middle Jurassic, rocks of the Quesnel arc were deformed during oblique collisions of the microcontinental Insular Superterrane (Monger et al., 1982) and then a massive oceanic plateau (Livaccari et al., 1981; Liu et al., 2010) that shuffled rocks along the ancestral continental margin, southward and then northward (Enkin, 2006; Sigloch and Mihalynuk, 2013). Quesnel, Stikine, and much of the Insular superterrane were finally pinned to North America by arc collisions in the Eocene (Bordet et al., 2013; Sigloch and Mihalynuk, 2013). Much of the southern Cordillera has since experienced extension (Brown and Journeay, 1987), giving rise to the landscape from which modern topography was inherited. Accurate reconstruction of the prolifically mineralized Late Triassic arc cannot be achieved without first restoring the effects of Jurassic to Eocene (and younger?) deformation.

Major volcanosedimentary successions of the Nicola arc (Fig. 4) were established through the pioneering works of Rice (1947), Schau (1968); Preto (1979) and Monger (1989), as compiled by Massey et al. (2005). They include the Nicola Group (Late Triassic), Spences Bridge Group (Early Cretaceous), Princeton Group (Eocene), and Chilcotin Group (Miocene-Pliocene). Most volcanic units have intrusive counterparts (Figs. 2, 3).

### 3. Nicola Group

Nicola Group strata in the Shrimpton Creek area belong mainly to the 'Central' and 'Eastern' belts of Preto (1979). Lithologies typical of the 'Western belt' have been mapped west of the Shrimpton area (Diakow and Barrios, 2008). Herein we focus on a transect across the northern part of the Shrimpton map area. From east to west, we recognize the Eastern belt (Preto, 1979) and subdivide much of the Nicola Group into the Eastern siliciclastic, Paradise, Shrimpton, and Harmon Lake successions, which define an overall trend from deep-water lithofacies to more arc-proximal lithofacies (Fig. 4). In the northwest part of the map area, the Harmon Lake succession includes the 'Shea polymictic conglomerate', the 'Voght unit' which consists of interbedded coarse bladed plagioclase porphyry flows and epiclastic redbeds, and is capped by 'Tillery' andesitic breccias (Fig. 4). Previous mappers assigned the

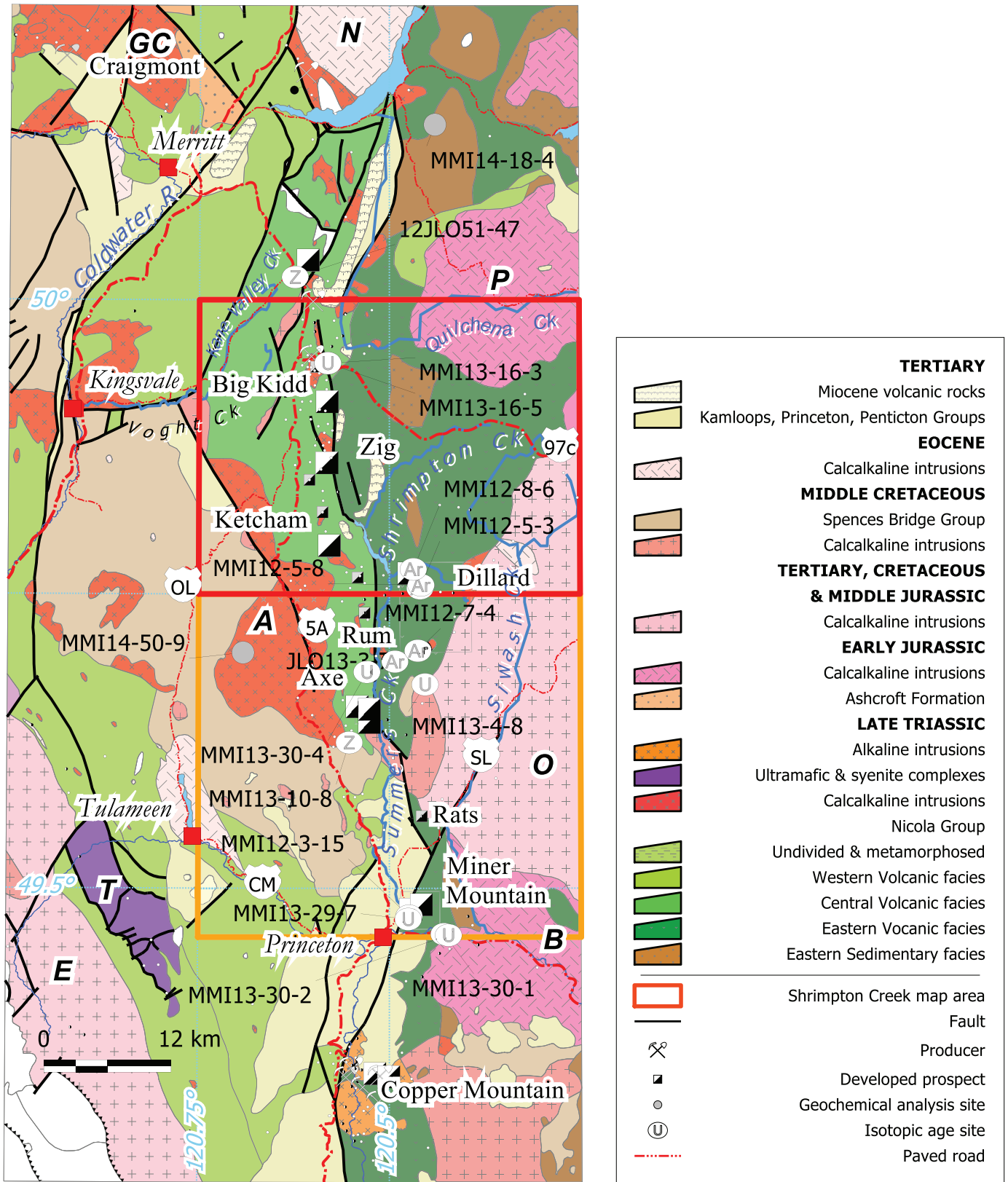
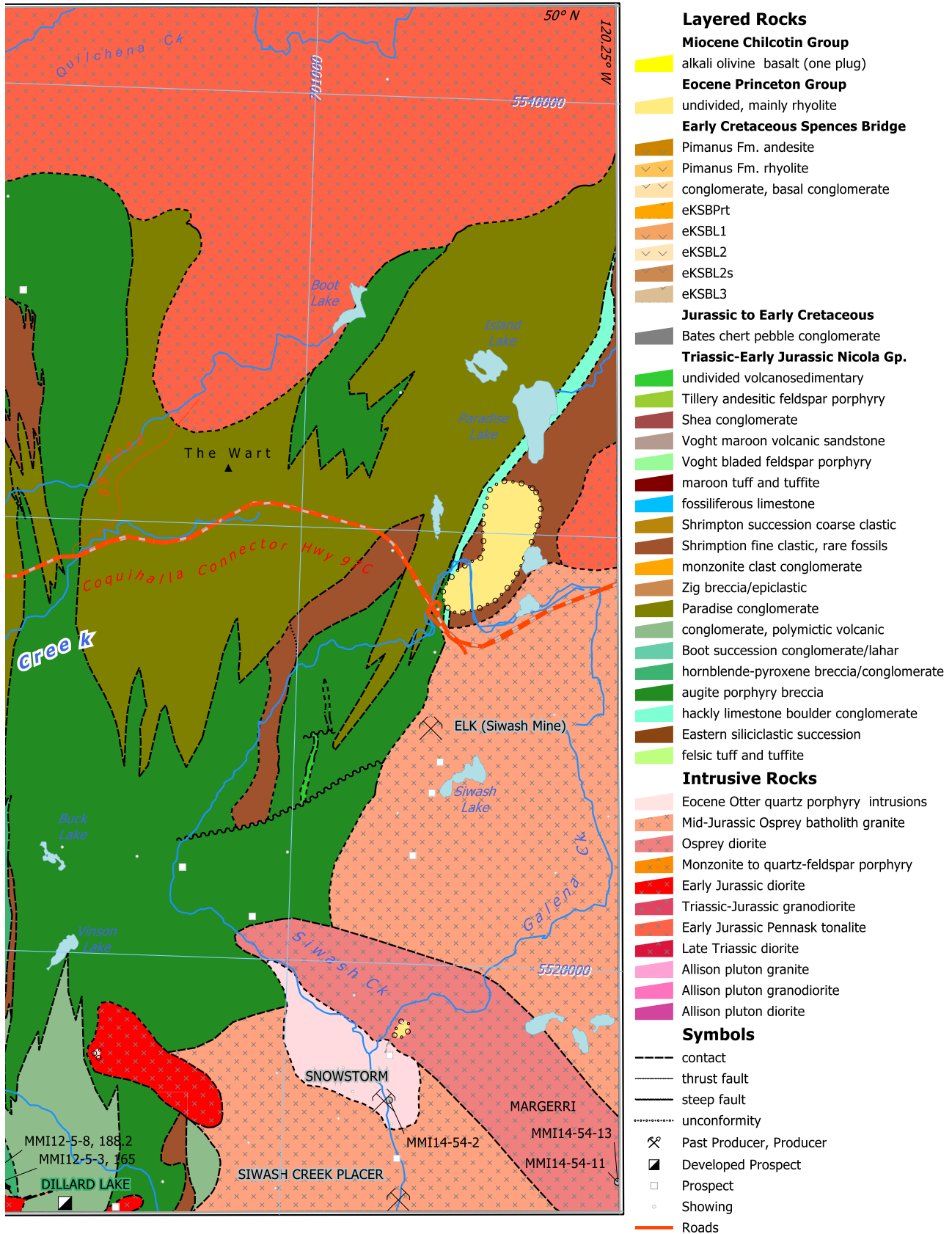
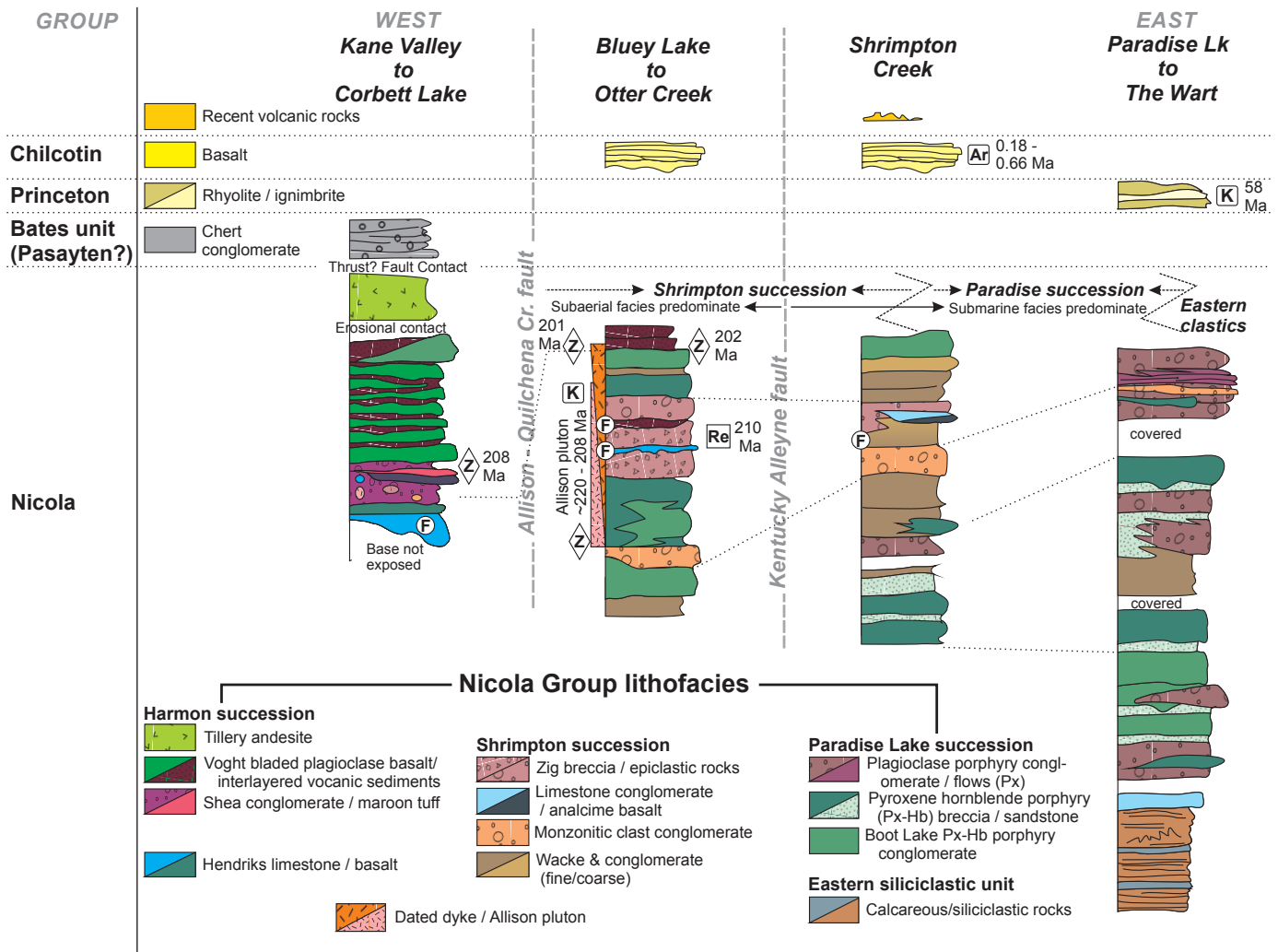


Fig. 2. Geological setting of field mapping, between Princeton and Merritt. Extents of Preto's (1979) Eastern belt (mafic submarine volcanic and sedimentary rocks), Central belt (arc axis, mafic volcanic and coeval intrusive rocks) and Western belt (intermediate to felsic volcanic and sedimentary rocks) are shown for reference, as adapted from Massey et al. (2005). Abbreviations denote major plutons: A = Allison Lake, B = Bromley, BI = Boulder intrusion, E = Eagle, GC = Guichon Creek, N = Nicola, O = Osprey Lake, P = Pennask, S = Summers Creek, T = Tulameen Complex. See Figure 1 for context. Orange box = 2013 mapping, red box = 2014 mapping.



**Fig. 3.** Simplified map of the Shrimpton Creek area. Compilation includes geological information from Monger (1989, regional framework), Preto (1979, mainly including areas between Shrimpton Creek and Highway 5A); Bergy (1999, PAR property); Gourlay (1991, ZIG property); and Nelson and Walker (1972, ZIG area).





**Fig. 4.** Stratigraphic relations in the Shrimpton Creek area. Shapes overprinted with F, Ar, K, Re and Z indicate age control: macrofossils (F, age determinations pending), and isotopic ages:  $^{40}\text{Ar}/^{39}\text{Ar}$  cooling age (Ar), K-Ar cooling age (K), Re-Os age (Re), and zircon detrital zircon ages (Z), or crystallization ages (Z on a black background). Older Allison Lake pluton ages are inferred from detrital zircons in overlying basal Early Cretaceous Spences Bridge conglomerate (cf. Mihalynuk et al., 2014).

Harmon succession to either the Upper Triassic (Monger, 1989) or Lower Cretaceous (Preto, 1979). New geochronology from the base of the succession (see below) establishes deposition in the Late Triassic to early Jurassic, at least 14 million years later than the youngest strata locally dated in the Nicola Group. The Harmon Lake succession lies unconformably above a carbonate unit of presumed Late Triassic age; herein named, the Hendriks limestone, and is faulted against younger, chert-rich conglomerate well exposed where incised by Bates Creek (unit 9 of Preto, 1979; unit Ks of Monger, 1989), and herein named the Bates conglomerate (Fig. 4).

In the eastern part of the map area, the Eastern fine siliciclastic succession is siltstone and sandstone that is capped by marble-clast-bearing conglomerate beds referred to herein as the ‘hackly carbonate unit’. This unit is stratigraphically overlain by the Paradise succession which, at its base, is a conglomerate and coarse sandstone unit derived from augite

and lesser hornblende-phyric mafic volcanic rocks. These strata pass upwards with gradual reduction in hornblende concentration into the main Paradise succession composed predominantly of medium-grained pyroxene-phyric mafic volcanic rocks interfingering with conglomerate derived from augite-feldspar-rich volcanic porphyries, and lesser monzonite-sourced conglomerate.

The Shrimpton succession gradationally overlies the Paradise succession, and is represented by predominantly immature volcanic-derived sandstone with locally intercalated monzonitic-clast conglomerate, and scant, thin flows of analcime-bearing basalt. A resistant subunit consisting mainly of monzonitic clasts can be mapped for kilometres. A unit similar in appearance, but containing distinctive grains of biotite, apatite and quartz, is well exposed around the Zig prospect (Fig. 3) and is herein called the ‘Zig unit’. Epiclastic strata containing clasts of Zig unit form mappable

layers in the Shrimpton succession which extends as far west as the Kentucky-Alleyne Fault (Fig. 3). West of this fault, in the Fairweather Hills (Fig. 3), basaltic flows, conglomerates and laharic breccias, interpreted as subaerial deposits, are the predominant Nicola Group lithologies (Lefebure, 1976). Although the current study conducted several traverses through the Fairweather Hills and found the conglomerates contained broadly similar lithologies as those in the Paradise succession, our work there is insufficient to reliably correlate with strata further east.

### 3.1. Eastern siliciclastic unit

Fine-grained siliciclastic strata were recognized east (Rice, 1947; Monger, 1989; Ray and Dawson, 1994) and south (Mihalynuk et al., 2014a) of the Shrimpton map area. We found that at least 410 m of these strata can be mapped on low ridges east of Paradise Lake, before they are lost eastward under cover or to intrusion of the Pennask batholith (Fig. 3). Batholith intrusion caused widespread thermal metamorphism, manifested mainly as bleaching of beds to shades of white and grey, increased induration and pyrrhotite disseminations.

Thin- to medium-bedded (0.5 to 30 cm thick) siltstone, sandstone, argillite and lesser granule to pebble conglomerate weather grey, white and rust. Medium-thick beds of sandstone with a calcareous matrix weather distinctively, but are a minor constituent. Shallow trough and ripple cross stratification are uncommon, although well-developed locally; most beds are parallel laminated and graded, commonly with scoured bases, typical of distal turbidites. Flame and ball and pillow structures are common and local zones of intense syndepositional disruption by gravity sliding and/or water escape are common (Fig. 5).

The hackly carbonate conglomerate unit forms the westernmost exposure of the Eastern unit. The conglomerate consists of spherical to tabular clasts up to boulder size. In some places, the clasts have weathered recessively leaving the hackly, sandy matrix behind (Fig. 6). Clasts are predominantly



**Fig. 5.** Irregular top of a ~0.4 m thick disrupted bed in the eastern sedimentary succession is the product of soft-sediment deformation.



**Fig. 6.** Carbonate clast-bearing conglomerate at the top of the eastern sedimentary succession. Carbonate clasts, up to boulder size, weather recessively relative to sandstone matrix, yielding a hackly appearance.

white, medium-crystalline marble; much less abundant are laminated, contorted siltstone and augite porphyry fragments, up to boulder size. Continuous outcrops expose a thickness of only ~8 m, but finer-grained conglomerates can be found across a covered interval that could overlie ~200 m of strata assuming persistent dips and no structural omission or duplication. Although the upper contact of conglomerate unit is not exposed, augite porphyry clasts and sandstone interbeds with pyroxene grains suggest a conformable transition to pyroxene and hornblende-bearing epiclastic rocks of the overlying Boot Lake unit of the Paradise succession.

The Eastern fine siliciclastic unit may be correlative with the Stemwinder Formation, which is relatively well constrained by microfossil ages as Late Carnian to Late Norian in age (Ray et al., 1993) and is interpreted to have been deposited in a back arc basin (Ray and Dawson, 1994).

### 3.2. Paradise Lake succession

Widespread in the northeastern quadrant of the study area, the Paradise succession crops out between younger batholiths, and it expands westward attaining a cross-strike breadth presumed to exceed 13 km. In northern and southeastern regions, the Pennask (Early Jurassic) and Osprey (Middle Jurassic) batholiths crosscut and locally metamorphose Paradise stratigraphy to pyroxene hornfels facies.

The lower part of the Paradise succession (referred to herein as the Boot Lake unit) consists mainly of hornblende-bearing conglomerate with fine clastic interbeds and sparse lava flows. The upper part of the Paradise succession underlies the region west and southwest of The Wart. Where coarse augite-phyric lava flows, a hallmark of the Nicola Group, predominate and are interleaved with lesser conglomerate and finer clastic rocks, they are included in the augite-phyric flow unit (see e.g., Mihalynuk et al., 2014),

The upper contact of the Paradise succession, observed locally

in the northwest, is gradational. Mafic flows are interlayered with sandstone that increases in proportion upsection into predominantly siliciclastic rocks of the Shrimpton succession. The age of the Paradise succession is uncertain. However, limestone clasts in conglomerate near the top of the unit might be derived, in part, from carbonate units in the Nicola Group west of Summers Creek Fault that contain conodonts of Late Carnian to Middle Norain age.

### 3.2.1. Boot Lake unit

The Boot lake unit comprises as much as one-third of the entire Paradise succession, and is exposed north of the Coquihalla Highway, between The Wart and the Eastern succession. Because of discontinuous outcrop, the thickness of the Boot Lake unit is uncertain. However, if the mainly west-dipping succession is not duplicated, it could be more than 4 km thick. The unit consists of conglomeratic and finer sedimentary strata composed predominantly of plagioclase and pyroxene with or without hornblende-phyric clasts (Fig. 7). In most places, the conglomerate forms massive layers composed of open framework cobbles and boulders, commonly with local bedded intervals of granule-size and finer clastic rocks. The clasts are mostly subangular to subrounded and are composed mainly of textural variants of fine- and medium-grained hornblende-augite plagioclase-phyric extrusive volcanic rock.

About 2 kilometres west of Paradise Lake, an interval more than 100 metres thick consists primarily of interbedded sandstone and siltstone with coarse augite and hornblende grains. A thin flow containing coarse hornblende prisms locally underlies a siltstone that contains a rare bivalve, which may indicate marine sedimentation. Higher in the section, conglomeratic beds reappear interlayered with sandstone; however, notably present are hornblende prisms, some up to 1 cm long, in the matrix and as clasts of hornblende-augite phyric mafic flows. Rare pebbles from a pyroxenite intrusion have also been observed. The clastic rocks are arranged in parallel



**Fig. 7.** Polymictic conglomerate of the Boot Lake unit containing only mafic, arc-derived clasts.

thin and thick beds with interlaminations and contain rip-up clasts at the base of some coarse sandstone beds. Channels in sandstone infilled with granule conglomerate grading to sandstone suggest stratigraphic younging toward the northwest.

### 3.2.2. Augite-phyric lava flows

Westward from The Wart for approximately 9 km to the inferred upper contact of the Paradise succession, the conglomerate generally lacks hornblende and comprises interbeds within more prominent lava flow sections. In this broad transect, the succession is particularly well exposed in newly harvested timber blocks along the west-facing slope of a prominent ridge trending north to its highest point at The Wart. Everywhere, the volcanic rocks consist of fine- and medium-grained porphyries containing plagioclase as the predominant phenocryst and ubiquitous augite, which is commonly altered to chlorite. The porphyritic texture and aphanitic groundmass of these volcanic rocks suggest a flow origin. Amygdaloidal flows occur at several isolated localities. At the northwestern extent of the Paradise succession, northwest of Pothole Creek, mafic flows occur exclusively; the conglomeratic beds pinch out farther southeast of this area.

Conglomerates west of The Wart differ from those between Paradise and Boot lakes only in the apparent greater clast diversity and significantly reduced or absent hornblende grains. Augite-plagioclase basalt porphyry flow remains the most abundant clast type, with the addition of pink fine-grained hornblende?-plagioclase phyric dacite and vesicular basalt clasts. Monzonitic clasts with fine-grained texture and brownish red color are abundant in exposures along Coquihalla Highway, from the point where the 88 Road passes under the highway, east towards The Wart summit (Fig. 3).

The southwestern extent of the Paradise succession in the Shrimpton Creek area is on a broad ridge between Buck and Missezula lakes. Here cobble-boulder conglomerate interlayered with coarse sandstone interbeds occupies a section inclined northwest that apparently overlies a thick sequence of augite-porphyry flows exposed to the southeast. Farther southwest towards Missezula Lake, a lateral lithologic change in the unit corresponds with the prevalence of hornblende-bearing clast conglomerate, locally associated with hornblende-augite-phyric lavas. Rare cobbles of grey limestone in conglomerate at three isolated localities between the Coquihalla highway and Missezula Lake may mark a stratigraphic level near the top of the Paradise succession.

We speculate the Paradise succession aggraded in a segment flanking the Nicola arc where relatively low relief prevailed. The clastic detritus, rich in mineral constituents and clasts resembling the flows were likely derived from immediately surrounding volcanic rocks and were presumably recycled and resedimented periodically (Fig. 8). The presence of more exotic clasts including porphyritic dacite, limestone and monzonite requires input from more distant sources that mixed with locally derived detritus.



**Fig. 8.** Orange-weathering augite-phyric autobreccia (under hammer) to conglomerate (left) transition demonstrates an immediately local source for some of the Paradise succession conglomerate facies.

### 3.3. Shrimpton succession

The Shrimpton succession is a predominantly siliciclastic unit consisting of: 1) feldspathic sandstone, granule- to cobble-conglomerate, siltstone, and siliceous argillite; 2) lenses of monzonite clast-bearing conglomerate; and 3) analcime-bearing lava flows (Figs. 9, 10). It is exposed mainly on ridges adjacent to Shrimpton Creek and extending north of the Coquihalla Highway to beyond Pothole Creek (Fig. 3). An easily accessed exposure showing the main lithologies of the succession is at the Loon Lake junction on the Coquihalla Highway. Here interlayered wacke, siltstone, argillite and impure limestone are folded and separated by high-angle faults from conglomerate with sparse monzonitic clasts.

The contact between the Shrimpton and Paradise successions is marked by a transition of interlayered mafic flows and sandstones; the base of the Shrimpton succession, exposed north of Pothole Creek is arbitrarily placed at the lowest sandstone interbed. The upper contact is also gradational and, east of Summers Creek, is presumed to be above a bed of monzonite clast-bearing conglomerate that is interleaved with clastic rocks containing mineral pyroclasts characteristic of the Zig unit.

#### 3.3.1. Feldspathic wacke and conglomerate

Feldspathic wacke, and conglomerate (Fig. 9a) are the most widespread components of the succession. Bedded sandstones north of Pothole Creek form continuous sections up to 450m thick in which beds dip moderately west-southwest. Farther south, exposures at the Coquihalla highway, Loon Lake Junction display strongly folded strata and outcrop-scale thrust faults (see below), introducing the possibility of larger contractional structures that have not been recognized in forested outcrops. Typically, siltstone and siliceous argillite occupy relatively thin, well-bedded intervals in otherwise massive, thickly bedded sandstones. Dark grey and black limestone is scarce, typically

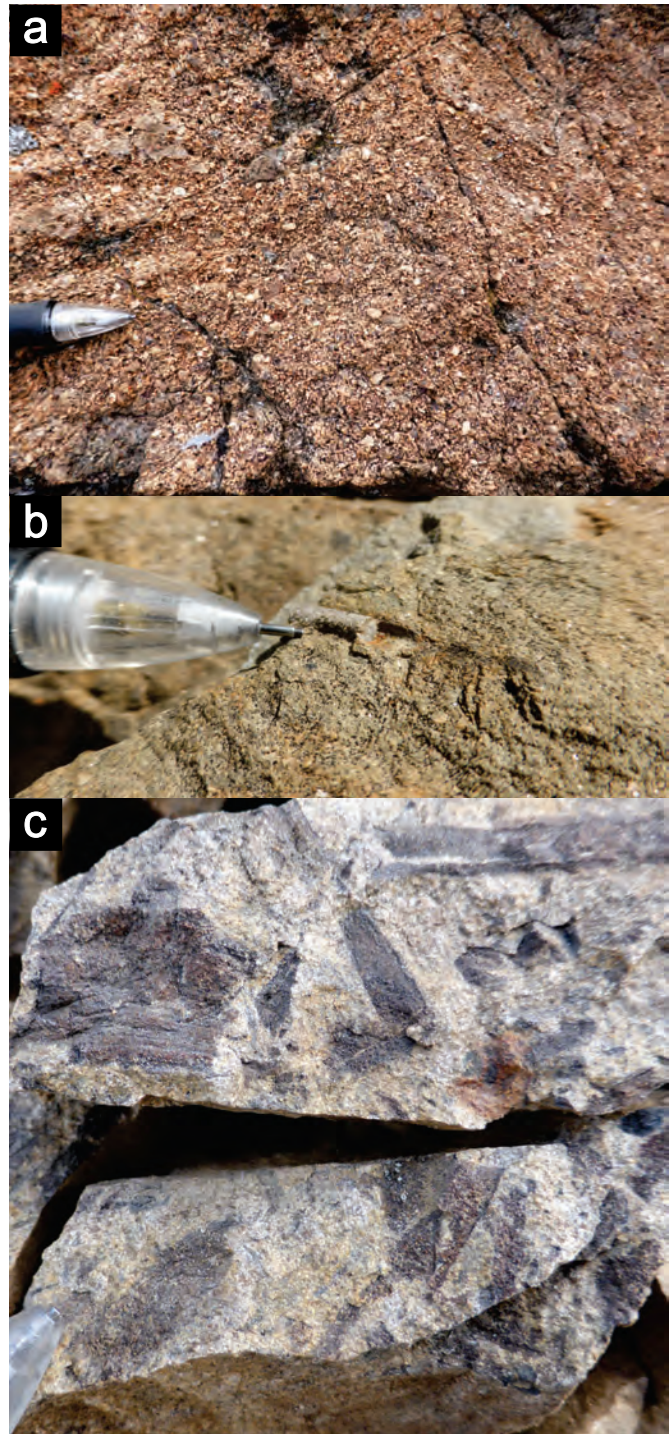


**Fig. 9.** Shrimpton succession. **a)** Pink-weathering, texturally and compositionally immature granule-conglomerate bed with mainly pink monzonitic debris. **b)** Crinoid stem in fine-grained calcareous sandstone. **c)** Medium-grained feldspathic wacke with carbonized plant debris.

in thin beds that locally contain fossils, including small bivalves, ammonoids, and crinoid stems that indicate marine sedimentation. Crinoids stems also occur in fine calcareous sandstone (Fig. 9b), in sections of coarser wacke containing

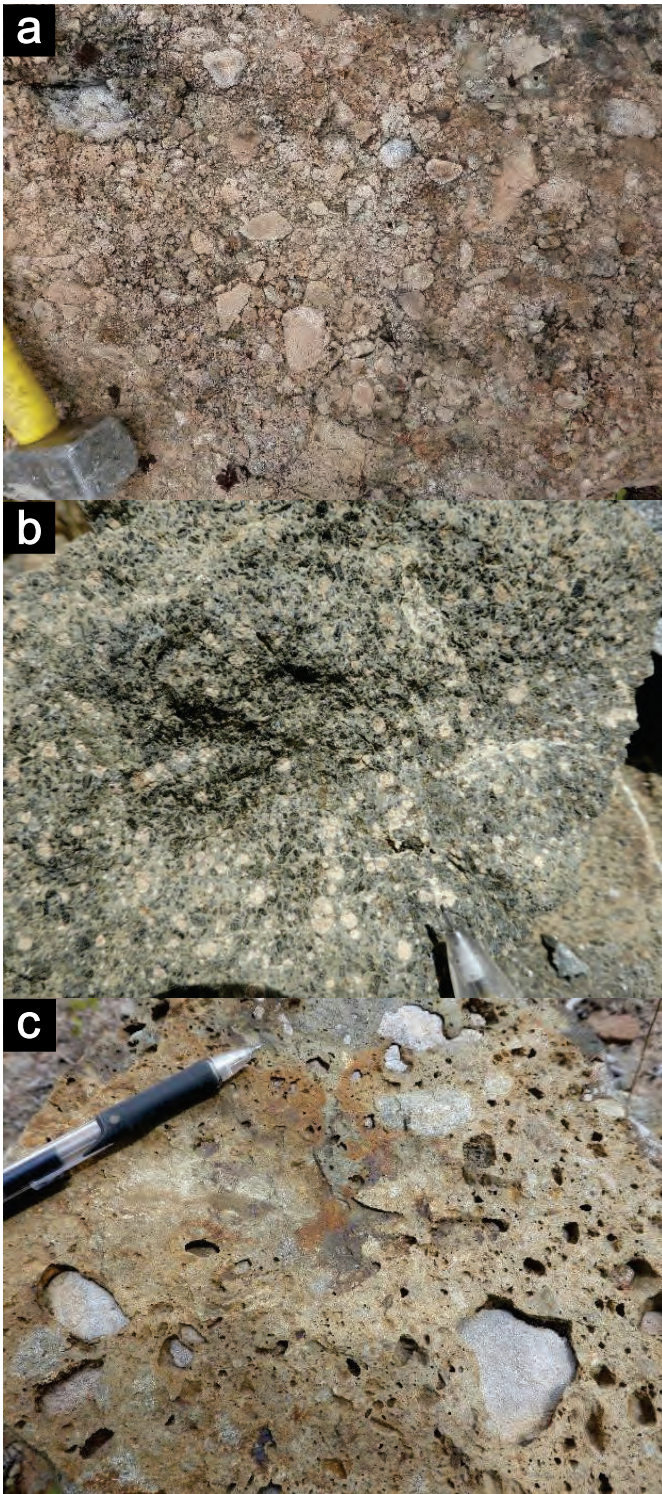


**Fig. 10.** a) Angular to rounded monzonitic clasts in Shrimpton succession conglomerate. b) Pyroxene (dark green to black) and analcime (rounded, light pink-tan) porphyry flow. c) Conglomerate interbed in Shrimpton sandstone, feldspar-rich sandstone matrix weathering in positive relief relative to limestone clasts.

locally abundant coaly layers with fossils of swamp grass (Fig. 9c), indicating transitional marine (brackish) deposition.

### 3.3.2. Monzonite clast conglomerate

East of Shrimpton Creek, local heights of land are underlain by resistant, massive conglomerate lenses conspicuously rich in pink to orange-weathering monzonitic clasts (Fig. 10a). One lens is up to 320 m thick and extends along strike for more than 10 km. Smaller lenses occur upsection, or as structural repeats. Upper and lower contacts of these conglomerate lenses grade into coarse sandstone. Rounded to angular monzonitic clasts are relatively uniform in composition and contain medium-grained, tabular feldspar that averages around 20%. The clasts are in a recessive ash-rich matrix that contains pyroxene, hornblende, biotite and rare quartz grains. Biotite occurs as medium-grained, golden, silver, or grey-green altered booklets, comprising as much as 4% of the rock, but typically less than 0.5%. Medium- to fine-grained quartz eyes are subhedral and smoky. They are irregularly distributed, typically sparse (<0.1%), but rarely can comprise as much as 2% of decimeter-thick layers. This unit appears to be the source of large glacial erratic boulder train 20 km to the south. A similar unit is distinguished by the presence of up to ~1%, fine- to medium-grained prismatic apatite. It is referred to as the 'Zig unit' (see below).

### 3.3.3. Analcime basalt flows

Analcime-pyroxene-phyric lava flows (Fig. 10b) just a few m thick are locally interleaved with sandstone and siltstone typical of the Shrimpton succession. Three isolated occurrences appear to occupy a specific interval west of the monzonitic clast conglomerate lenses. Locally adjacent to the flows are carbonate layers and conglomerates containing angular carbonate boulders (Fig. 10c). Intercalation of analcime pillow breccia and tuffaceous layers of estimated dacite to trachyte composition indicates synchronous sedimentation and at least some submarine arc volcanism, raising the possibility of volcanogenic massive sulphide accumulations. Sparse sulphide pebbles composed mainly of pyrrhotite and pyrite with traces of chalcopyrite are conspicuous constituents of resistant sedimentary units capping the ridge immediately east of the Kentucky-Alleyne Fault at Bluey Lake.

### 3.3.4. Zig unit

The Zig unit consists of variably reworked heterolithic breccia and lapilli tuff with continuously exposed thicknesses in excess of 150 m. The unit is the main host to mineralization at the Zig prospect immediately west of Bluey Lake. Diagnostic of Zig unit volcanic rocks are biotite, quartz, and red apatite prisms that combined usually comprise <2 % of rock matrix, with more abundant medium-grained tabular feldspar and fine-grained pyroxene. Volcanic clasts vary from red to dark green, very fine-grained or aphanitic. Possible hypabyssal accidental fragments are light pink holocrystalline monzonite, hornblende diorite and rare hornblende-biotite ?lamprophyre. Locally, the unit is strongly bleached and displays epidote alteration; pyroxene is typically replaced by chlorite, and fine-grained idiomorphic magnetite crystals are oxidized to hematite. Near the Nor 30 occurrence, the unit includes muddy maroon tuffite

that contains angular to well-rounded pebbles and cobbles of conspicuous diorite clasts representing up to 20% of the clast population, as well as sparse limestone clasts. Irregular beds of siltstone to arkosic sandstone and maroon mudstone are common. Sand grains are composed of plagioclase, lesser pyroxene and rare olivine(?). Fine-grained magnetite, replaced by hematite locally, comprises as much as 15% of the matrix. These magnetite-rich beds continue laterally for up to 400 m and may be more than 5 m thick. Poor sorting, weak clast alignment, and contorted bedding within this subunit are most consistent with deposition primarily as laharic flows.

### 3.3.5. Age of the Shrimpton succession

Tuffaceous sandstone layers interpreted to be near the top of the Shrimpton section contain biotite, apatite, and quartz and are interpreted as remnants of pyroclastic fallout associated with the Zig unit. If this correlation is correct, the age of the upper part of the Shrimpton succession may be ~210 Ma, the Re-Os age of mineralization associated with the Zig unit (unpub. data). Biochronology of the Shrimpton succession is pending identification of several ammonoid specimens and prospective conodont samples obtained from two limestone localities in the lower part of the succession.

### 3.4. Fairweather Hills laharic breccia and conglomerate

Ridges east of Highway 5a and west of Kentucky-Alleyne Fault, between Miner Lake in the south and Tule Lake in the north cover an area referred to as the Fairweather Hills. Here, Upper Triassic Nicola strata were mapped in detail at 1:6,000-scale as part of a M.Sc. thesis (Lefebure, 1976), following previous work by Christopher (1973) and Preto (1974). During this study we elected to not duplicate this earlier mapping, conducting traverses only to the edges of the Fairweather Hills, and isolated spot checks.

Lefebure (1976) shows Nicola stratigraphy broken by primary longitudinal block faults and smaller transverse faults. Across the longitudinal structures are significant changes in Nicola group facies and thickness. A medial fault block is underlain by mafic flows and lahars, interbedded in sub-equal amounts, with a cumulative thickness estimated at 1100 m. In flanking fault blocks, thicknesses decrease; to the east, lahars are predominant and to the west, lahars are interlayered with volcanic conglomerate, sandstone, and minor limestone. Mafic flows contain varying proportions of plagioclase and augite phenocrysts, as porphyries and amygdaloidal varieties, commonly accompanied by autoclastic breccia. Lahars in the medial block contain clasts mainly of augite-plagioclase basalt porphyry with abundant monzonitic and locally dioritic intrusive rocks. The lahars to the east contain mainly andesite and basalt porphyry, and lesser diorite clasts. To the west, basaltic rocks are predominant, with few sedimentary clasts. In general, these laharic deposits show poor sorting of mainly rounded to subrounded clasts.

### 3.5. Hendriks limestone

Typically massive white and light grey to tan-weathering, fossiliferous limestone attains thicknesses of at least 240 m along both sides of the Kane Valley. Bedding is locally distinct where intercalated with arc detritus, basalt flow or hyaloclastite debris, and dips away from the valley axis, which is slightly oblique to the broad, faulted, anticlinal hinge (Fig. 3). Upper parts of the unit, particularly south of the Tillery Road, contain bivalve-rich micritic limestones with exquisite fossil preservation, or reworked fossils in coquinas. Colonial coral heads more than a metre across can be discerned, especially where recrystallization is weakest, south of Tillery Road. Identification of fossils collected is pending.

The limestone is intercalated with volcanic rocks and conglomeratic lenses derived from volcanic terrain. One volcanic flow unit occupies a consistent position near the top of the limestone. It is a grass green aphanitic basalt flow and flow breccia with poorly developed pillows. Abundant fine chlorite amygdales are characteristic. Hyaloclastitic debris of the same composition form planar interbeds with the limestone.

Hendriks limestone has not been traced northeast or southwest beyond exposures in the Kane and Voght valleys. It appears that it was removed in both directions below a regional unconformity.

Siliciclastic rocks at the base of the overlying Harmon succession yield a detrital zircon maximum depositional age of about 208 Ma (see below). This age also establishes the Hendriks limestone as older, and presumably of Late Triassic age. The nearest Upper Triassic limestone outcrop to the Hendriks limestone is about 6.5 km to the north-northeast (Diakow and Barrios, 2008). It can be traced an additional several km farther north to near Sugarloaf Mountain where Preto (1979) mapped it as one of multiple limestone beds that locally contain early Norian fossils. This limestone section is succeeded above by a thin quartz-bearing dacite tuff from which a U-Pb zircon crystallization age of ~224 Ma was recently obtained (Diakow, unpub. data). If a provisional correlation is made between limestones near Sugarloaf Mountain and Kane Valley, they are somewhat older, and potentially bracket a hiatus in Nicola Group deposition, represented by the unconformable surface on the Hendriks limestone, between ~224 and ~208 Ma.

### 3.6. Harmon succession

The Harmon succession is a new stratigraphic division proposed for semi-continuous, sedimentary and volcanic strata. Where thickest northeast of Harmon Lake, it is conservatively estimated to be more than 2 km thick. Conglomeratic strata at the base of the succession comprise the lowest of four lithostratigraphic units. Here called the 'Shea conglomerate', it is thought to underlie a significant part of the valley bottom, apparently thickest at Shea Lake; however outcrops are few and widely spaced. Overlying units are: a lower undivided andesitic volcanic unit, 'Voght' bladed-plagioclase basalt porphyry flows and sandstone, and the 'Tillery' andesite unit.

The Harmon succession was included as part of Lower

Cretaceous stratigraphy (Preto, 1979), and as previously mapped, extends north of the Shrimpton Creek map area to Mount Nicola. Geological mapping by Monger (1989) assigned this succession to the Upper Triassic Nicola Group, including it within the Central belt. We interpret that the succession is confined between regional unconformities, the lower cuts into Hendriks limestone with a presumed Late Triassic age, and the upper is overlain by a chert conglomerate unit, herein named Bates conglomerate, possibly of Middle Jurassic to Early Cretaceous age.

### 3.6.1. Shea conglomerate

Oxidized, reddish maroon polymictic granule to boulder conglomerate is locally in direct contact with mafic flow rocks intercalated with the Hendriks limestone. Its thickness is highly variable, generally thicker and more widespread in Kane Valley and from Shea Lake area southward in Voght Valley, and very thin or absent in faulted blocks adjacent to Voght Creek and the Tillery Road.

Typically poorly sorted, the clasts are oxidized red and well rounded, varying from pebbles to boulders, and consisting of diverse lithologies that include: augite and hornblende-bearing volcanic porphyries; aphanitic and flow-laminated rhyolite and welded tuff; white and grey massive and sparsely fossiliferous limestone; monzonite, granodiorite, diorite and granite; and scarce chert and argillite. Except for chert, all of the clasts resemble lithologies found nearby in the Nicola Group or Late Triassic comagmatic plutonic phases. Undoubtedly, the conglomerate represents erosion of Nicola Group stratigraphy. In addition, boulders containing the distinctive mineral components characteristic of the Zig formation are recognized.

Sandstone and conglomeratic layers composed of granule and pebbles occur throughout massive, coarse conglomerate, generally as discontinuous spaced interbeds displaying parallel stratification and graded structure. Shea conglomerate is intercalated with maroon, mostly aphanitic to finely feldspar-phryic lapilli ash tuff.

Rare exposure of coarse-grained, pyroxene-plagioclase porphyry lava flow forms an interlayer locally or directly underlies Shea conglomerate. This flow, well exposed in a Coquihalla Highway cut across from Corbett Lake, consists of 40 m of coarse pyroxene-plagioclase-phryic and amygdaloidal basalt that is sharply overlain by Shea conglomerate with sandstone interbeds. It is distinguished by up to 30% plagioclase laths between 3-5 mm (locally >1 cm) long, and 2-5% pyroxene up to 3 mm diameter. Amygdaloidal texture, imparted by rounded and irregular white crystalline quartz amygdales, occurs only at the base and in a reddish oxidized zone at the top, which identifies the volatile-rich margins of a solitary flow. Lava displaying identical texture, observed at a locality in the Kane Valley, is considered to overlie Shea conglomerate which crops out about 5m lower, with the contact concealed in a grassy slope. Clasts of bladed-feldspar basalt porphyry observed in the Shea conglomerate might be derived from these lavas.

### 3.6.2. Lower, undivided andesitic volcanic rocks

This unit comprises andesitic lava flows, and minor sandstone and lesser conglomerate. Although the outcrops are small and isolated, they consistently occupy a general position topographically higher than Shea conglomerate and below overlying distinctive bladed plagiophryic flows. Thickness of the unit varies along strike, suggested by apparent thinning towards the north, and absence of correlative strata in faulted stratigraphy near Tillery Road. The unit is at least 350 m thick, based on an approximate contact with underlying Shea conglomerate and overlying bladed-plagioclase basalt porphyry.

Mainly andesite flows with porphyritic and amygdaloidal textures, the unit contains 15-25% plagioclase between 1 and 3mm long, and 1-3% pyroxene phenocrysts up to 1.5mm that locally display red oxidation. The amygdaloidal rocks also contain similar phenocrysts, in addition to rounded and irregular quartz amygdales. Conglomeratic beds contain rounded cobbles and smaller clasts apparently derived from andesitic volcanic rocks.

### 3.6.3. Voght bladed plagioclase basalt porphyry flows and clastic rocks

Multiple, bladed-feldspar porphyry lava flows forming resistant ridges, locally separated by interflow sandstones, overlie the lower andesite unit. The unit is exposed on both sides of the Kane Valley. The best exposures are on the southeast valley side where recessive sandstone generally identified by red soil and angular chips marks the base of a lava succession containing at least 13 successive flows. The flows range in thickness from <5 to ~70 m and the unit might have a cumulative thickness of as much as 850 m.

The lowest flow member is the coarsest, with euhedral plagioclase laths up to 1.5 cm and larger glomerocrysts randomly dispersed in a dark green-black groundmass (Fig. 11 a). Passing up through this flow there is a gradual reduction in the length of plagioclase laths to between 4-7 mm and an overall increase in abundance to around 25-30%. Finer grained pyroxene phenocrysts typically account for less than 10%. Vesiculation is quite variable throughout; most are filled by laumontite and commonly rimmed by chlorite. The highest flow unit mapped contains relatively rare amygdales, composed either of white opalescent or crystalline quartz, that are up to 5 mm diameter, and sparse medium-grained plagioclase in a very finely felted to aphanitic blue-green groundmass. Upper parts of this highest unit show an oxidized, deep red colour (Fig. 11b). Rare exposures of maroon epiclastic beds immediately above some flow units include concentrations of scoraceous bladed-porphyry fragments.

Poorly exposed red-brown laminated and graded sandstone and siltstone occupy intervals up to 20 m thick between successive lavas. Interflow conglomerate with bladed-porphyry clasts is exposed at one locality in west Kane Valley (Fig. 11c). A sill origin for some of these flows was suspected by Preto (1979); however, there is no evidence of thermally

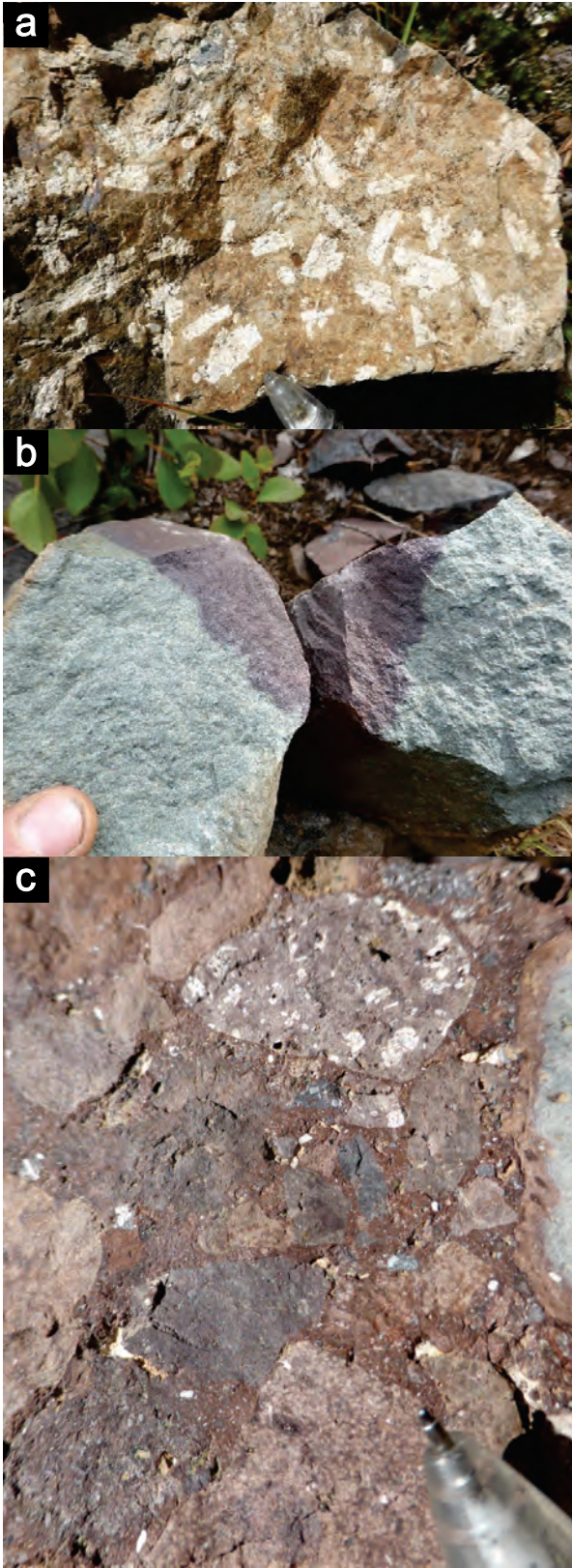


**Fig. 11.** Harmon succession, Voght unit bladed porphyry unit. **a)** Lowest flow, with very coarse bladed plagioclase. Plagioclase grain size decreases upsection. **b)** Highest flow with hematite staining. **c)** Intraformational conglomerate includes cobbles of coarse bladed feldspar porphyry.

altered interflow sediments, as might be expected by a massive injection of basalts.

The bladed-plagioclase basalt porphyry, although distinctive, is not restricted to the Harmon succession. Basalts with similar texture and overall appearance also have been observed at the base of the basal Shea conglomerate. In the Nicola Group, bladed-plagioclase basalt flows are not uncommon. For example, in the Paradise succession, they accompany highly vesiculated lavas in an area south of the Elkhart junction on the Coquihalla Highway (Fig. 3). Boulders also occur in conglomerate near the Axe deposit (Fig. 2).

#### 3.6.4. Tillery andesites

The uppermost unit of the Harmon succession consists of fine- and medium-grained andesite porphyry and amygdaloidal lava flows, and relatively minor conglomerate and sandstone. Inclusion of this unit at the top of the Harmon succession is based on the relationship between a solitary exposure composed of underlying Voght strata that are abruptly replaced upsection by extensive andesite lava flows. The unit name originates from the general region of Voght Creek and the Tillery Road, where it is most extensive. North of the Tillery Road, the unit wedges out and has been removed by a combination of erosion and reverse faulting (Fig. 3), resulting in its absence in the homoclinal section east of Harmon Lake. Tillery andesites are unconformably overlain by Bates conglomerate, as exposed on an east-facing slope south of the Tillery Road.

Lava flows displaying fine and medium porphyritic and amygdaloidal textures comprise most of the unit. The porphyritic flows contain 20-30% plagioclase generally less than 3mm long, and rare pyroxene phenocrysts. Amygdaloidal flows generally form thin members in the more prevalent porphyritic flows, however, they predominate in eastern exposures of the unit, attaining an estimated thickness of more than 400 m near the contact with overlying Bates conglomerate, south of Tillery Road. Amygdaloids in the rock consist mainly of white quartz and an unidentified white zeolite with radiating habit. Uniform, fine- and medium-grained tabular feldspar porphyry breccia (Fig. 12) occurs locally as do conglomerate and sandstone layers. The conglomerate contains mainly cobbles of plagiophytic flows, like those that characterize the Tillery unit. Near the base of the unit, are dense vitreous, banded flows up to 4 m thick. Rare feeder dikes to these flows display highly irregular margins.

Data to directly constrain the minimum age of the Tillery andesite are lacking.

#### 3.7. Nicola Group interpretation

Early workers recognized that Nicola volcanic arc rocks are flanked to the east and west by sedimentary strata (Campbell, 1966; Schau, 1968). The Shrimpton Creek area lacks evidence of an underlying basement like the Harper Ranch Group to the north, near Kamloops, which comprises mainly erosional relicts of a Late Devonian to Late Mississippian arc (Beatty et al., 2006). To the east, the Chaperon Group has been interpreted



Fig. 12. Harmon succession, Tillery unit feldspar porphyry breccia.

as a narrow Permian rift deposit formed on attenuated North American crust and correlative to the Harper Ranch Group (Thompson et al., 2006). To the south, the Anarchist Group (Middle Devonian to Early Permian) is interpreted as an 80 to 90 m.y. record of mid ocean ridge basalt to intra-oceanic tholeiitic arc formation (Massey and Dostal, 2013), strongly contrasting with the interpreted paleotectonic setting of the Chaperon Group.

Thus far, our detrital zircon analyses have failed to reveal a single Precambrian zircon, more consistent with an intraoceanic arc than with a continental arc origin. If an intra-oceanic arc setting is correct, distal background sedimentation was likely pelagic, overwhelmed by input from the emergent Nicola arc, and increasingly more volcanic and less sedimentary in character with proximity to the arc axis. Remarkably fresh tuffaceous sediment containing euhedral pyroxene, hornblende and olivine (see Boot Lake succession) indicate little residence time between original pyroclastic deposition, erosion and redeposition. Almost all primary volcanic units, such as coarse flow breccias or flows, are intercalated with sedimentary rocks, some of which contain marine fossils, unequivocal evidence of submarine deposition.

At least three erosional surfaces can be identified in the Nicola arc in the Shrimpton Creek area: above the Hendriks limestone, overlain by the Shea conglomerate of probable Late Norian age; above the Voght volcanic sandstone unit, approximately at the Triassic-Jurassic boundary; and above the Tillery andesite unit, probably sometime in the Early Jurassic. All may be correlative with similar erosional events observed along the length of the Quesnel and Stikine arcs (e.g. Logan and Mihalynuk, 2014).

#### 4. Bates conglomerate

Massive tabular beds of distinctive, well-rounded black chert granule to boulder conglomerate comprise the Bates unit. Poorly developed beds are typically decimetres to a few metres thick with rubbly black surfaces that commonly display a weak, rusty red patina. The Bates unit is at least 420 m thick and extends from near Courtney Lake, ~17 km southwards to where it is beveled off by the modern erosional surface near the uplifted northern margin of the Late Triassic Allison Lake pluton. About 10 km farther south, the Spences Bridge Group

(Early Cretaceous) directly overlies the Allison Lake pluton without any intervening Bates unit rocks.

Only in some of the northern exposures, near Tinmilsh Lake, do cobbles and boulders of lithologies other than black chert comprise a significant proportion of the unit, including altered light grey granitoid and dark green volcanic rocks and black siltstone. Here the unit weathers orange, probably due to carbonate alteration, and is faulted and interleaved with well-cleaved argillite and siltstone. Except for these northern outcrops, which probably represent the lowest exposed parts of the unit, the predominance of chert clasts suggests a very restricted source region, with no contribution from currently local sources. A widespread source of chert is unknown in the Shrimpton Creek area. Cache Creek complex to the west and Slocan Group to the east are both sources of chert that may have been exposed during orogenesis in the Middle to Late Jurassic (see “Structure” below).

#### 5. Spences Bridge Group (Early Cretaceous): Lodwick succession

The Spences Bridge Group is exposed over an area of 50 km<sup>2</sup> west of Highway 5A (Figs. 2, 3), where it is conterminous with a broader northwest-trending volcanic field at Shovelnose Mountain to the northwest (Diakow and Barrios, 2008), and southeast towards Princeton (Mihalynuk, et al. 2014a). Herein we mainly use stratigraphic nomenclature from Thorkelson and Rouse (1989) and Diakow and Barrios (2009).

We use the informal name ‘Lodwick succession’ for sections of the Pimainus Formation, (the basal unit of the Spences Bridge Group) best exhibited in the general vicinity of Lodwick Lake.

The Lodwick sequence is subdivided into three distinctive subaerially erupted rock units, which collectively conform to a regionally consistent eruptive pattern, albeit with local variability, that is observed throughout the Early Cretaceous volcanic tract between Princeton and Shovelnose Mountain. Initial volcanic deposits consist of an andesitic flow unit (Unit eKSBL1), succeeded sequentially by two felsic units (Units eKSBL2 and eKSBL3). The lower felsic unit consists of a solitary rhyodacitic pyroclastic flow and associated epiclastic deposits, conformably overlain by a dacitic flow unit. The Coalmont Road transects this sequence, and particularly good sections of the felsic components and related sedimentary rocks are adjacent to the road descending into, and forming the cliffs of Otter Creek valley.

Because of the scattered nature of small exposures comprising the andesite unit, its overall thickness is indeterminate; however, consistent spatial relationships confirm that it is stratigraphically lower than the felsic units. In general, the felsic units and associated epiclastic deposits thicken progressively to the northwest, attaining a maximum thickness at Otter Creek valley. Where the Coalmont Road crosses Otter Creek, dacite flows of the uppermost unit (Unit eKSBL3) form prominent columnar joints in cliffs more 75 m high. Nearby, these flows appear to abut the underlying rhyodacite ash-flow tuff and interfinger with epiclastic rocks, across a steep depositional contact.

Towards the northwest, beyond Otter valley, the felsic units either disappear or thin dramatically. This geometry suggests that the felsic units preserve a synvolcanic paleochannel. The dacite flow unit is restricted to several thin outliers outcropping nearby, and presumably resting conformably on the underlying andesite unit.

### 5.1. Andesites (Unit eKSBL1)

Andesitic lava flows and scant lapilli interbeds that comprise this unit typically weather to small, widely spaced, solitary outcrops. Distribution of these rocks extends from low-relief terrain along the western margin of the Allison pluton at Highway 5A westward to higher elevation near Lodwick Lake, where the upper contact with overlying rhyodacitic ashflow tuff is observed at one location. In the east, andesite exposures are scattered over 5 km close to granitic rocks of the Allison pluton, although contacts are not exposed. However, at nearby Gladstone Lake, andesite flows distributed over about 1 km<sup>2</sup> and surrounded by plutonic rocks presumably represent an outlier unconformable on the Allison pluton. In glacially sculpted terrain covered by thick till north of Otter Creek, midway between Highway 5A and the Coalmont Road, isolated andesite outcrops protrude through till close to topographically higher outcrops of chert-bearing conglomerate. Although the contact is concealed, it is interpreted as a steeply inclined sub-andesite unconformity that cuts into the Bates conglomerate unit (see above).

The flows are olive green, and typically display porphyritic textures imparted by 20–25% medium-grained plagioclase and up to several percent pyroxene (partly replaced by chlorite). Amygdaloidal varieties, locally with white opalescent silica amygdules, are rare. West of the Coalmont Road, andesites differ from those farther southeast near the Allison pluton in that flow breccia is more widespread and generally associated with oxidized maroon lavas containing an earthy green mineral, tentatively identified as celadonite, and chalcedonic silica infilling fractures and small cavities. These flows closely resemble those of unit PS1 comprising the basal flows of the Pimainus Formation in the adjoining Shovelnose Mountain area (Diakow and Barrios, 2008).

### 5.2. Rhyodacite lapilli tuff and derived epiclastic rocks (Units eKSBL2 and eKSBL2s)

Felsic volcanic fragmental and epiclastic rocks make up this unit. Widely distributed throughout the Johnny-Thalia-Lodwick lakes area, the relative volume of the epiclastic rocks apparently exceeds that of the tuffs. Here, the epiclastic rocks contain rock and crystal detritus that is similar to pyroclasts found in the tuffs. Although these tuffs continue northward to Otter Creek, the interlayered epiclastic rocks apparently terminate on the south side of the valley.

#### 5.2.1. Rhyodacite tuff (Unit eKSBL2)

Unit eKSBL2 depositionally overlies andesitic rocks of unit eKSBL1 north of Lodwick Lake. The unit consists

predominantly of dacitic to rhyodacitic lapilli tuffs and rare rhyolitic ash tuff and laminated flows. These tuffs display a light green matrix that supports a variety of lithic fragment types. Most fragments are angular and subangular <3 cm to 10 cm in diameter, although block-size fragments occur (particularly in some eastern exposures). The clasts consist of varicolored, fine-grained volcanic porphyries and fewer, but diagnostic, flow-laminated and aphanitic dacite-rhyolite, collapsed pumiceous rhyolite, and pinkish fine- to medium-grained granitic rocks, some of which resemble phases of the Allison pluton. Also diagnostic are trace to 2% quartz and biotite. The tuff commonly contains m-scale interbeds of pebble conglomerate and sandstone with local parallel stratification.

The tuff unit is believed to have originated as a pyroclastic flow that has undergone minimal compaction. These rocks closely resemble unit PS4, a thick and widespread mainly pyroclastic unit at Shovelnose Mountain (Diakow and Barrios, 2008).

#### 5.2.2. Conglomerate and sandstone (Unit eKSBL2s)

Conglomerate with sandstone interbeds underlie tuffs of unit eKSBL2 east of Lodwick Lake. This clastic unit thickens westward where conglomerate interfingers with tuff. Conglomerate forms thick, massive beds composed mainly of poorly sorted, polymictic and matrix-supported clasts. The clasts vary from subangular to well-rounded cobbles and sparse boulders that can reach 45 cm diameter (typically <20 cm). Planar bedded sandstone, locally with abundant carbonaceous plant debris, and granule-pebble layers form m-thick interbeds.

A conglomeratic and sandstone succession, lithologically distinct from that near Lodwick Lake, is faulted against andesite of unit eKSBL1 at its northern extent, adjacent to the Coalmont Road. Sandstone and siltstone from this unit underlie and, in part, interfinger with tuffs of unit eKSBL2 farther south in the Otter Creek valley. The conglomerate is a massive layer more than 30 m thick with self-supporting poorly sorted angular and subrounded boulders (up to 1.5 m in diameter). The clasts consist of andesite, porphyritic dacite and abundant flow-laminated rhyolites. Bedded sandstone and siltstone containing thin carbonaceous-rich layers occurs locally above the deposit.

This coarse clastic bed appears to locally overlie a comparatively finer siliciclastic sequence exposed in a series of cuts along the Coalmont Road. The sequence displays dark green, planar beds and characteristic weathering to rounded surfaces with conchoidal fracturing. It is composed of thickly bedded granule-pebble conglomerate alternating with medium and coarse sandstone and thinly bedded and interlaminated siltstones. The sandstones are composed mainly of plagioclase, some pyroxene and rare quartz. Structures in the rocks include graded bedding, small-scale channels, and ball and pillow structures. Plant debris is widespread in the finer grained layers, including rare tree stems up to 5 cm in diameter.

Based on the stratigraphic position relative to felsic tuffs and similar clast lithologies, the conglomerates in the vicinity of Lodwick Lake correlate with unit PS2 of the Pimainus

Formation at Shovelnose Mountain (Diakow and Barrios, 2008). A comparison of the siliciclastic units north of Otter Creek valley with those to the south near Lodwick Lake, indicates they occupy the same relative stratigraphic position, although significant lithologic differences exist, implying differing provenance. Conglomerates in the south contain clasts identical to lithic and crystal fragments found in tuffs of unit eKSBL2, implying periodic erosion and resedimentation of tuff deposits. In addition, the presence of ubiquitous granitic clasts in Unit eKSBL2 (see above) suggests a potential source for minor granitic detritus in conglomerates of unit eKSBL2s. North of Otter valley the finer clastic components contain sparse pyroxene, which may have been derived from andesites near the base of the Spences Bridge Group. The coarse boulder conglomerate contains abundant flow-laminated rhyolite, probably derived locally from voluminous flows in the Pimainus Formation at Shovelnose Mountain.

### 5.3. Dacite flow (Unit eKSBL3)

Dacite lava flows comprise the uppermost unit of the Spences Bridge Group in the Lodwick succession. The distribution and thickness of the unit is influenced by differential uplift in blocks separated by three steeply dipping north-south faults. Most widespread in the central block, the unit is continuous, forming cliffs north of Thalia Lake to Otter Creek valley. Conservatively estimated to be between 30 and 80 m thick in this segment, the flow unit dramatically thins north of the Otter Creek valley. The east-west extent of the unit is limited by a sub-horizontal outlier covering about 5 km<sup>2</sup> in the western block and it abruptly terminates at the fault marking the margin of the eastern block.

The lower contact of the unit is consistent throughout the region as a shallow, north-inclined plane, sharply separating the dacite from underlying unit eKSBL2 tuffs and eKSBL2s epiclastic rocks. On the northwest side of Thalia Lake, the contact is marked by a 2 m-thick hornblende-dacite porphyry flow not seen elsewhere in the unit. This distinctive flow directly overlies thinly bedded quartz and biotite-bearing unit eKSBL2s sandstone.

The dacite is remarkably uniform in appearance, typically forming cliffs exhibiting columnar joints. It weathers orange, and breaks into either blocky or slab-like pieces. The porphyritic texture is diagnostic, imparted by 15-20% subhedral feldspar up to 4 mm long and fewer feldspar glomerocrysts distributed evenly throughout the groundmass. Mafic minerals might be present as greenish anhedral grains in the rock; however, they are too small to identify macroscopically. Thin laminated flows were observed locally.

Although the dacite is generally unaltered, at a solitary location in a 50 m<sup>2</sup> area, fresh chalky clay minerals replace plagioclase phenocrysts and the groundmass. Where this alteration increases in intensity the porphyritic texture is obliterated, thereby yielding a dense off-white rock that is easily confused with an aphanitic rhyolite. White and translucent banded chalcedony, some with a central open cavity lined with

drusy quartz, comprise rare veinlets observed crosscutting the dacite flows.

Massive dacite has not been mapped elsewhere in the Spences Bridge Group. It may represent a solitary flow that exhibits pronounced thinning northwest over 7 km, suggesting that the vent might originally have been located farther south in an unmapped area. Based on the present distribution of the dacite, an inferred general flow path towards the northwest appears to coincide with a distinctive flow laminated rhyolite (unit PS6) which presently forms a broad lobe extending from higher elevation on Shovelnose Mountain, towards the southeast to its present terminus within 1 km of the closest dacite outlier. Because of their close proximity we speculate that these felsic flows once coalesced and are temporally equivalent.

## 6. Princeton Group (Eocene)

Only a few outliers of Princeton Group volcanic rocks are exposed in the Shrimpton Creek map area. The largest of these is between the western map boundary and McCullough Creek (west of Davis Lake, Fig. 3). These rocks apparently rest on an unconformity above the Spences Bridge Group to the west and in possible fault contact with the Allison pluton to the east. Smaller erosional remnants occur in the northeastern map area where they are mainly shallowly dipping, sparsely amygdaloidal rhyodacitic flows. Princeton Group volcanic strata are well dated near Princeton (Ickert et al., 2009) as between 53 and 47 Ma, (early part of Eocene, Cohen et al., 2013).

### 6.1. Rhyodacite flow outliers

Except where well-exposed in roadcuts, outcrops of rhyodacite flows form low-relief, tan to light grey and platy weathering, glacially sculpted mounds. Flows are very fine-grained to aphanitic with sparse, medium-grained feldspar phenocrysts and glomerocrysts. Vesicles are typically sparse and are locally filled with a soft, amber-coloured mineral along with chlorite and chalcedonic quartz. Some vesicles are not infilled by mineral matter.

### 6.2. Quartz-biotite rhyolite

Quartz-biotite-phyric ash flow crops out in two restricted areas in the eastern Shrimpton Creek area. South of Vinson Lake, a probable intrusive unit with a matrix lithologically similar to the ash flows is interpreted as a feeder.

White-weathering outcrops contain smoky quartz as fractured and rounded eyes (up to 20%); vitreous medium-grained plagioclase (up to 25%); orthoclase as altered, chalky white, medium-grained crystals (up to 15%) and sparse megacrysts to 1 cm diameter; and fine- to medium-grained golden to black biotite (3%). Beautiful flow banding of a white, ash-rich matrix locally contains ~3 % flattened and weakly welded grey pumice lapilli. Sparse accidental granodiorite fragments (Fig. 13) confirm that the tuff postdates crystallization of the adjacent batholith, from which the fragments were most likely derived.

Roadbed outcrops between Dillard and Vinson Lakes are



**Fig. 13.** Princeton Group. Quartz-eye, biotite-bearing rhyolite with accidental fragments of granodiorite.

lithologically similar to the ash flow, but lack flow banding and fragmented crystals, and are much coarser grained, with up to 15% coarse smoky quartz eyes and 5-20% euhedral anorthite crystals up to 3 cm by 10 cm. These textural differences are attributed to an intrusive origin, likely a feeder of the ash flows. As constrained by the distribution of rhyolite porphyry and surrounding granitic outcrops, the feeder is more than 65 m, but less than 1100 m in diameter.

### 7. Miocene to Recent basalt

Two ages of young basaltic flows occur in the Shrimpton Creek area: pre- and post- Quaternary.

Basalt flows infilling paleovalleys that have been inherited by the modern Shrimpton Creek-Missezula Lake and the Kentucky-Alleyne drainages, are capped by Quaternary deposits in which glaciated boulders derived from the flows can be a predominant component. Most extensive of these basalt units are horizontal, massive to columnar jointed flows, typically 2 to 5 m thick. They display scoraceous, brecciated bottoms with vesicle content decreasing toward the flow center. Vesicle pipes are common. Green to amber, medium to coarse olivine phenocrysts with irregular and commonly iridescent fractures comprise up to 1% of the rock. A very fine mat of plagioclase with interstices filled by black glass, or coated by glass that surrounds angular void spaces, are typical matrix types. Similar flows units occur as sporadic relicts in the Summers Creek area where they have been more fully described by Mihalynuk et al. (2014a), and are correlated with the Chilcotin Group of Miocene to Pliocene age (Mathews, 1989). They have been isotopically dated in the Coalmont area (Fig. 2) as 9 and 9.2 ± 1.8 Ma (Late Miocene; Mathews, 1989; recalculated by Breitsprecher and Mortensen, 2004), but those are apparently much older than rocks in the Shrimpton Creek area, which have  $^{40}\text{Ar}/^{39}\text{Ar}$  step heating plateau ages of 0.2 ± 0.5 to 0.66 ± 0.03 Ma (Sluggett, 2008). Such young ages confirm the relative age assignments of the older “plateau” and “valley basalts” by Rice

(1947). Here we follow the usage of Rice (1947) and include all intra-glacial basalt flows as “valley basalt”. Recent basalts are treated separately.

Recent basalt occurs as highly scoraceous blocky tuff and spatter less than a m thick that are irregularly distributed atop about one hectare of Quaternary till and gravels east of Shrimpton Creek. Spatter cements the gravel that it came into direct contact with. Some granitic clasts entrained in the spatter fused to crystal mush with a quenched glass matrix. Droplets and mm veneers of spatter coat boulders; some granitoid boulders display spalled spatter rinds. Charcoal remains of trees are preserved where they were engulfed in scoraceous flow (Fig. 14), and imprints of other burnt organic matter, including growth rings, record where these organic materials have eroded away. No evidence of a vent was found; however, where the unit appears thickest it has been disturbed during construction of a logging landing, and any relict of a vent may have been infilled.

### 8. Intrusive units

Intrusive rocks in the study area include Late Triassic to Middle Jurassic plutons (Fig. 3) and dikes interpreted as coeval with Spences Bridge Group volcanic rocks (late Early Cretaceous). Late Triassic intrusions along the axis of the central Nicola belt, (as defined by Preto, 1979) include the polyphase Allison pluton (204 ± 10 to 207 ± 10 Ma, K-Ar hornblende and muscovite cooling ages in Preto, 1979; recalculated by Breitsprecher and Mortensen, 2004; and detrital zircons in Mihalynuk et al., 2014b) in the southwest part of the Shrimpton Creek map area, and numerous undated dioritic bodies such as at the Big Kid and Ketchan prospects, all interpreted as part of the ~205 Ma Copper Mountain suite (Logan and Mihalynuk, 2014). The northeastern and eastern parts of the study area are underlain by the Pennask batholith (Early Jurassic; 194 ± 1 Ma) and western parts of the Osprey Lake K-feldspar megacrystic granite batholith (166 ± 1 Ma;



**Fig. 14.** Highly scoraceous Recent basalt with charcoal wood fragments (pen tip).

U-Pb zircon ages from Parrish and Monger, 1992; and the ~160-164 Ma ages from zircons reported here). An extensive, north-trending dike swarm in the Summers Creek map area is correlated with the 104 Ma Spences Bridge Group to the west (Diakow and Barrios, 2009) and the 'Mine dikes' along strike to the south at Copper Mountain ( $103 \pm 0.3$  Ma, Mihalynuk et al., 2010; also known as 'Candy Stripe dikes'). This correlation is confirmed by geochronology (see below) but these dikes are largely unknown in the Shrimpton Creek area. One possible exception is east of Shrimpton Creek where a restricted, weak swarm of dikes with the same mineralogy, and up to ~10 m thick, are mapped north of Buck Lake (too small to show on Fig. 3). A series of quartz-feldspar porphyry dikes and stocks that cut the Osprey Lake batholith and are associated with gold mineralization at the Siwash mine, have returned K-Ar cooling ages that cluster around 53 Ma (Armstrong and Peto, 1981 and Hunt and Roddick, 1990; recalculated in Breitsprecher and Mortensen, 2005).

### 8.1. Allison pluton

The Allison pluton underlies the southwest corner of the Shrimpton sheet where it is nonconformably overlain by the Spences Bridge Group (Figs. 2, 3). It is a composite body consisting of northeast-trending zones in which diorite and granite predominate.

Felsic phases range from pink, coarse-grained granite with smoky quartz, to medium-grained, white-weathering tonalite. Mafic phases range from quartz diorite (Fig. 15a) to hornblende-plagioclase pegmatite (Fig. 15b), and tend to be varitextured. Younger phases tend to be more felsic, but irregular contacts between mafic and felsic phases, chilling of mafic against felsic phases (Fig. 15c), and zones with abundant mafic enclaves in granitic phases, suggest comingling of melts.

### 8.2. Pennask batholith

White-weathering, medium- to coarse-grained hornblende-biotite granodiorite to tonalite of the Pennask batholith (Fig. 16) crops out across the northeast corner of the map area (Figs. 2, 3). Wide spaced joints, up to 1 or 2 m in places, create blocky outcrops on scarps, or gently rounded outcrops on glaciated surfaces. Plagioclase (30-50%), orthoclase (<20%) and quartz (30-40%) can be subidiomorphic, relatively fresh biotite forms medium to coarse booklets and intergranular mats and is generally more abundant than hornblende (8-15% combined). Hornblende may appear dusty due to incipient chlorite alteration and is locally subtrachytic, outlining an igneous flow fabric. Fine-grained magnetite and fine to medium-grained titanite comprise 1-2% and 0.5% of the rock respectively.

### 8.3. Osprey Lake batholith

The Osprey Lake batholith covers more than 1100 km<sup>2</sup> between Peachland and the southwest corner of the Shrimpton map area (only ~95 km<sup>2</sup> are in the map area). Granite is the most common phase, forming white to pinkish-grey, rounded to blocky outcrops. K-feldspar megacrysts comprise 20 % of



**Fig. 15.** a) Pegmatitic hornblende diorite. One of a series of northeast-trending zones in the Allison pluton. b) Foliated dioritic border phase of the Allison pluton includes rafts of foliated diopside skarn, and is cut by synkinematic dikelets of quartz diorite. c) Cuspate-lobate contact between comagmatic diorite and granodiorite, Allison pluton.



**Fig. 16.** Typical salt and pepper Pennask tonalite, here with minor grey-green fault planes lined by chlorite.

the rock over broad areas. They are up to 5 cm long, and may display growth zones outlined by hornblende microlites; they tend to have light-coloured rims. Medium- to coarse-grained plagioclase, orthoclase, grey quartz, biotite and hornblende comprise the matrix. Plagioclase and pinkish matrix K-feldspar comprises ~60% of the rock volume. Biotite forms 3-5 mm euhedral to subhedral books comprising ~10% of the rock, and medium-grained hornblende is ~6%. Accessory minerals identifiable in hand sample include euhedral, honey brown titanite (0.5-1%) and magnetite. Enclaves of hornblende diorite are common. Magnetic susceptibilities range between 20 and  $38 \times 10^{-5}$  SI. A strong thermal-metamorphic halo 0.5 km or more wide is developed around this massive body.

#### 8.4. Spences Bridge “Mine dikes”

An extensive set of dikes trends north, subparallel to the western contact of the Bromley pluton (Fig. 2). They are porphyritic, with phenocrysts of K-feldspar, plagioclase, quartz and chloritized hornblende in varying combinations. Some dikes are 10 m or more thick and have been interpreted as co-genetic with the Bromley pluton. On the basis of composition and a preliminary U-Pb isotopic age determination, Mihalynuk et al. (2014b) suggested a correlation between the ‘Mine dikes’ and Spences Bridge Group, a correlation confirmed by further U-Pb geochronology (see below).

#### 8.5. Otter intrusions

A coarse orthoclase-quartz porphyritic intrusion extending northwest from the confluence of Galena and Siwash Creeks, underlies about 5 km<sup>2</sup>. Most parts of the intrusion are pyritic, clay altered, and weather white, yellow and rust. In many localities hematite occurs as fine disseminations and pseudomorphically replaces octahedra of magnetite. The intrusion appears to be gradational with lithologically similar parts of the Osprey batholith, but is part of much younger east-trending belt of stocks that have yielded K-Ar ages of ~53 Ma

(Hunt and Roddick, 1990; Armstrong and Peto, 1981). Dikes included with the Otter intrusions cut the Osprey batholith at the Siwash mine and are interpreted as syn-mineralization.

### 9. Geochronology

Presented here are completed isotopic analyses on zircons extracted from samples collected during mapping: four analyzed by U-Pb isotopes by Chemical Abrasion-Thermal Ionization Mass Spectroscopy (CA-TIMS), and two analyzed by Laser Ablation (LA) ICP-MS. Geochronological results for 15 samples collected during fieldwork in 2014 are pending.

#### 9.1. Methodology

Abridged methodologies are presented here. Complete procedures are reported in the references cited and in companion publications (Mihalynuk et al., 2014b; Mihalynuk et al., 2015).

#### 9.2. Zircon CA-TIMS

CA-TIMS procedures described here are modified from Mundil et al., 2004, Mattinson, 2005 and Scoates and Friedman, 2008. Rock samples undergo standard mineral separation procedures; zircons separates are handpicked in alcohol. The clearest, crack- and inclusion-free grains are selected, photographed and then annealed at 900°C for 60 hours. Annealed grains are chemically abraded and then spiked with a <sup>233-235</sup>U-<sup>205</sup>Pb tracer solution (EARTHTIME ET535), and then dissolved. Resulting solutions are dried and loaded onto Re filaments (Gerstenberger and Haase, 1997).

Isotopic ratios are measured by a modified single collector VG-54R or 354S thermal ionization mass spectrometer equipped with analogue Daly photomultipliers. Analytical blanks are 0.2 pg for U and 1.0 pg for Pb. U fractionation was determined directly on individual runs using the ET535 mixed <sup>233-235</sup>U-<sup>205</sup>Pb isotopic tracer. Pb isotopic ratios are corrected for fractionation of 0.23%/amu, based on replicate analyses of NBS-982 reference material and the values recommended by Thirlwall (2000). Data reduction employed the Excel™-based program of Schmitz and Schoene (2007). Standard concordia diagrams are constructed and regression intercepts, weighted averages calculated with Isoplot (Ludwig, 2003). All errors are quoted at the 2σ or 95% level of confidence, unless otherwise noted. Isotopic dates are calculated with the decay constants  $\lambda^{238}=1.55125E^{-10}$  and  $\lambda^{235}=9.8485E^{-10}$  (Jaffe et al, 1971). EARTHTIME U-Pb synthetic solutions are analysed on an on-going basis to monitor the accuracy of results.

#### 9.3. Zircon LA-ICPMS

Zircons analyzed using laser ablation (LA) ICP-MS methods, employ techniques as described by Tafti et al. (2009). Instrumentation at the PCIGR comprises a New Wave UP-213 laser ablation system and a ThermoFinnigan Element2 single collector, double-focusing, magnetic sector ICP-MS. All zircons greater than about 50 microns in diameter are picked from the mineral separates and were mounted in an epoxy puck along with several grains of the Plešovice (337.13 ± 0.13 Ma,

Sláma et al., 2007), and Temora2 (416.78 ±0.33 Ma) zircon standards and brought to a very high polish. Prior to analysis, the surface of the mount was washed for 10 minutes with dilute nitric acid and rinsed in ultraclean water. The highest quality portions of each grain selected for analysis are free of alteration, inclusions, or possible inherited cores. Line scans rather than spot analyses are employed in order to minimize elemental fractionation during the analyses. A laser power level of 40% and a 25 µm spot size are used. Backgrounds are measured with the laser shutter closed for ten seconds, followed by data collection with the laser firing for approximately 35 seconds. The time-integrated signals are analysed using Iolite software (Patton et al, 2011), which automatically subtracts background measurements, propagates all analytical errors, and calculates isotopic ratios and ages. Corrections for mass and elemental fractionation are made by bracketing analyses of unknown grains with replicate analyses of the Plešovice zircon standard. A typical analytical session at the PCIGR consists of four analyses of the Plešovice standard zircon, followed by two analyses of the Temora2 zircon standard five analyses of unknown zircons, two standard analyses, five unknown analyses, etc., and finally two Temora2 zircon standards and four Plešovice standard analyses. The Temora2 zircon standard was analysed as an unknown in order to monitor the reproducibility of the age determinations on a run-to-run basis. Final interpretation and plotting of the analytical results employed the ISOPLOT software of Ludwig (2003).

#### 9.4. Geochronology results

Geochronology results for four CA-TIMS and two LA-ICPMS analyses are presented in Figures 17 to 21, and Tables 1 to 8. Complete raw data tables, cathode luminescence imagery of zircons, and ancillary plots such as those that show detrital zircon isochrons can be found in Mihalynuk et al., 2015. Most of the results are for samples collected in 2013 and only a cursory description of the units sampled is presented here. For more detailed descriptions see Mihalynuk et al. (2014a).

##### 9.4.1. Missezula Mountain rhyolite: Sample MMI13-30-4

Sample MMI13-30-4 (Table 1; Fig. 17) was collected from pyritic felsic lapilli tuff on the east flank of Missezula Mountain. It was a second attempt to date the unit; only a few zircon fragments were obtained from a more massive ignimbritic section to the south (“rusty rhyolite lapilli tuff” in Mihalynuk et al., 2014a), and they provided inconclusive results.

An age of 238.1 ±0.3 Ma is calculated based upon two overlapping fractions on concordia. Slightly discordant older grains may include an inherited older zircon component. To our knowledge, this is the oldest isotopic age obtained from the Nicola Group volcanic rocks. Felsic strata in the western belt tend to cluster around 224 Ma (Diakow, unpub data).

##### 9.4.2. Dike in Voght unit redbeds: Sample MMI13-16-5

Sample MMI13-16-5 (Table 2; Fig. 18a) was collected from a fine-grained dike that cuts red volcanic sandstone (Fig. 18b).

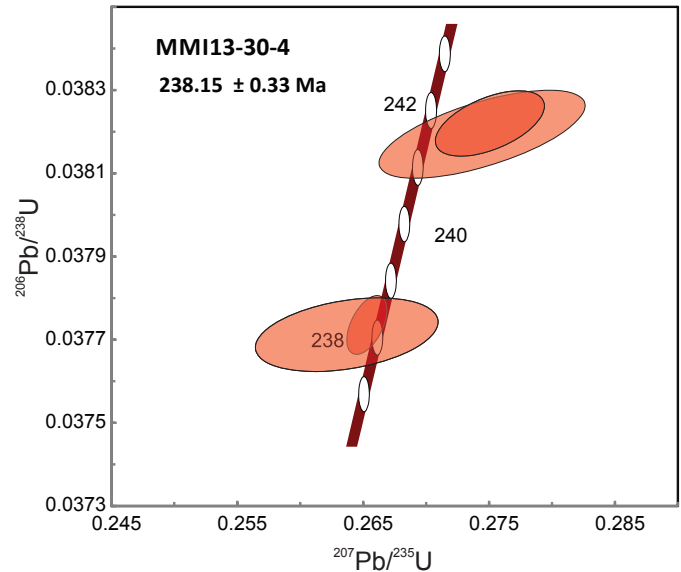


**Fig. 17.** Thermal Ionization Mass Spectrometric (TIMS) analysis of zircon U-Pb from sample MMI13-30-4 of felsic lapilli tuff on Missezula Mountain. An age of 238.1 ±0.3 Ma is based on two overlapping fractions on concordia. Slightly discordant older grains may include an inherited zircon component. Data point error ellipses are 2σ.

Four grains were run and these overlap concordia at 201 and 199 Ma. The more precise age is obtained from the older 2-grain cluster at 201 +0.3/-0.4 Ma; however, a circa 199 Ma age is also consistent with the age of the enclosing strata with a detrital zircon maximum depositional age (DZMD) of 202 ±4 Ma (see MMI13-16-3, below).

##### 9.4.3. Bromley pegmatite: Sample MMI13-30-1

Sample MMI13-30-1 (Table 3; Fig. 19) Bromley pluton does not crop out in the Shrimpton Creek map area. However, we include new geochronological data from the southeast Summers Creek map area (Fig. 2) from pegmatitic dikes that are presumably related to the main medium-grained, hornblende-biotite granodiorite pluton. These dikes cut the biotite hornfels halo that extends ~500 metres away from the pluton (garnet occurs within a few tens of metres of the contact). Pegmatite dike intrusion appears to have been synchronous with extensional faulting within the thermometamorphic halo, and, on the basis of widespread Tertiary extension across the Summers Creek map area, the pegmatite was assumed by Mihalynuk et al. (2014a) to be Eocene. However four zircons extracted from the pegmatite, all clustering on concordia, yield an integrated age of 193.6 ±0.3 Ma. This is the same age (within error) as a previous U-Pb age determination of the Early Jurassic Bromley pluton (193 ±1 Ma, Parrish and Monger, 1992).

##### 9.4.4. Mine dike swarm at Similkameen River: Sample MMI13-30-2

Sample MMI13-30-2 (Table 4; Fig. 20) is from a swarm of north-trending quartz-feldspar porphyry dikes (Fig. 20a). This



**Table 3. U-Th-Pb isotopic data for sample 30-1.**

Sample	Compositional Parameters										Radiogenic Isotope Ratios						Isotopic Ages								
	Wt.	U	Pb	Th	$^{206}\text{Pb}^*$	mol %	Pb*	Pb <sub>c</sub>	$^{206}\text{Pb}$	$^{208}\text{Pb}$	$^{207}\text{Pb}$	$^{206}\text{Pb}$	$^{207}\text{Pb}$	$^{206}\text{Pb}$	$^{207}\text{Pb}$	$^{206}\text{Pb}$	$^{207}\text{Pb}$	$^{206}\text{Pb}$	$^{207}\text{Pb}$	$^{206}\text{Pb}$					
	mg	ppm	ppm	ppm	$\times 10^{-13}$ mol		(pg)	(pg)			% err	$^{238}\text{U}$	% err	$^{235}\text{U}$	corr.	% err	$^{238}\text{U}$	% err	$^{235}\text{U}$	corr.	% err	$^{238}\text{U}$	% err	$^{235}\text{U}$	
(a)	(i)	(j)	(i)	(b)	(c)	(c)	(c)	(c)	(d)	(c)	(f)	(e)	(f)	(e)	(f)	(g)	(f)	(e)	(f)	(g)	(f)	(g)	(f)	(g)	(f)
<b>MM113-30-1</b>																									
C	0.0009	931	26.2	0.031	1.0678	99.68%	82	0.29	5868	0.010	0.050512	1.672	0.212824	1.656	0.030558	0.384	0.076	218.61	38.68	195.92	0.73	194.04	0.73	194.04	0.73
D	0.0008	459	13.1	0.030	0.4670	99.28%	36	0.28	2585	0.010	0.050257	1.527	0.211531	1.550	0.030527	0.271	0.174	206.90	35.40	194.84	0.52	193.84	0.52	193.84	0.52
E	0.0002	3198	93.5	0.042	0.8124	98.69%	20	0.90	1410	0.013	0.050089	0.873	0.210430	0.911	0.030469	0.131	0.354	199.13	20.27	193.91	0.25	193.49	0.25	193.49	0.25
F	0.0002	955	28.5	0.015	0.2427	97.92%	12	0.42	889	0.005	0.049899	1.547	0.209706	1.609	0.030480	0.261	0.313	190.29	35.99	193.31	0.50	193.55	0.50	193.55	0.50

(a) A, B etc. are labels for fractions composed of single zircon grains or fragments; all fractions annealed and chemically abraded after Mattinson (2005) and Scoates and Friedman (2008).  
 (b) Model Th/U ratio calculated from radiogenic  $^{208}\text{Pb}/^{206}\text{Pb}$  ratio and  $^{207}\text{Pb}/^{235}\text{U}$  age.  
 (c) Pb\* and Pbc represent radiogenic and common Pb, respectively; mol %  $^{206}\text{Pb}^*$  with respect to radiogenic, blank and initial common Pb.  
 (d) Measured ratio corrected for spike and fractionation only. Mass discrimination of 0.25%/amu based on analysis of NBS-982; all Daly analyses.  
 (e) Corrected for fractionation, spike, and common Pb; up to 0.9 pg of common Pb was all assumed to be procedural blank:  $^{206}\text{Pb}/^{204}\text{Pb} = 18.50 \pm 1.0\%$ ;  $^{207}\text{Pb}/^{204}\text{Pb} = 15.50 \pm 1.0\%$ ;  $^{208}\text{Pb}/^{204}\text{Pb} = 38.40 \pm 1.0\%$  (all uncertainties 1-sigma).  
 (f) Errors are 2-sigma, propagated using the algorithms of Schmitz and Schoene (2007) and Crowley et al. (2007).  
 (g) Calculations are based on the decay constants of Jaffey et al. (1971).  $^{206}\text{Pb}/^{238}\text{U}$  and  $^{207}\text{Pb}/^{206}\text{Pb}$  ages corrected for initial disequilibrium in  $^{230}\text{Th}/^{238}\text{U}$  using  $\text{Th}/\text{U}$  [magma] = 3.  
 (h) Corrected for fractionation, spike, and blank Pb only.  
 (i) Nominal fraction weights estimated from photomicrographic grain dimensions, adjusted for partial dissolution during chemical abrasion.  
 (j) Nominal U and total Pb concentrations subject to uncertainty in photomicrographic estimation of weight and partial dissolution during chemical abrasion.

**Table 4. U-Th-Pb isotopic data for sample MM113-30-2.**

Sample	Compositional Parameters										Radiogenic Isotope Ratios						Isotopic Ages								
	Wt.	U	Pb	Th	$^{206}\text{Pb}^*$	mol %	Pb*	Pb <sub>c</sub>	$^{206}\text{Pb}$	$^{208}\text{Pb}$	$^{207}\text{Pb}$	$^{206}\text{Pb}$	$^{207}\text{Pb}$	$^{206}\text{Pb}$	$^{207}\text{Pb}$	$^{206}\text{Pb}$	$^{207}\text{Pb}$	$^{206}\text{Pb}$	$^{207}\text{Pb}$	$^{206}\text{Pb}$					
	mg	ppm	ppm	ppm	$\times 10^{-13}$ mol		(pg)	(pg)			% err	$^{238}\text{U}$	% err	$^{235}\text{U}$	corr.	% err	$^{238}\text{U}$	% err	$^{235}\text{U}$	corr.	% err	$^{238}\text{U}$	% err		
(a)	(i)	(j)	(i)	(b)	(c)	(c)	(c)	(c)	(d)	(e)	(f)	(e)	(f)	(e)	(f)	(g)	(f)	(e)	(f)	(g)	(f)	(g)	(f)	(g)	(f)
<b>MM113-30-2</b>																									
A	0.0069	95	1.7	0.325	0.4440	97.34%	11	1.00	694	0.105	0.048478	1.740	0.108545	1.859	0.016239	0.169	0.728	122.65	40.97	104.63	1.85	103.84	1.85	103.84	1.85
B	0.0054	174	3.1	0.402	0.6355	97.90%	14	1.12	880	0.130	0.048627	0.960	0.109044	1.027	0.016264	0.144	0.522	129.90	22.57	105.09	1.03	104.00	1.03	104.00	1.15
C	0.0061	104	1.8	0.384	0.4307	97.61%	12	0.87	775	0.123	0.048001	1.206	0.107446	1.289	0.016235	0.141	0.620	99.30	28.53	103.63	1.27	103.81	1.27	103.81	1.15
D	0.0053	145	2.6	0.357	0.5206	96.92%	9	1.36	600	0.116	0.048814	1.501	0.109463	1.587	0.016264	0.203	0.480	138.92	35.23	105.47	1.59	104.00	1.59	104.00	0.21
E	0.0041	213	3.9	0.453	0.5928	97.48%	12	1.26	734	0.146	0.048578	2.021	0.109048	2.122	0.016281	0.268	0.431	127.53	47.54	105.09	2.12	104.11	2.12	104.11	0.28

(a) A, B etc. are labels for fractions composed of single zircon grains or fragments; all fractions annealed and chemically abraded after Mattinson (2005) and Scoates and Friedman (2008).  
 (b) Model Th/U ratio calculated from radiogenic  $^{208}\text{Pb}/^{206}\text{Pb}$  ratio and  $^{207}\text{Pb}/^{235}\text{U}$  age.  
 (c) Pb\* and Pbc represent radiogenic and common Pb, respectively; mol %  $^{206}\text{Pb}^*$  with respect to radiogenic, blank and initial common Pb.  
 (d) Measured ratio corrected for spike and fractionation only. Mass discrimination of 0.25%/amu based on analysis of NBS-982; all Daly analyses.  
 (e) Corrected for fractionation, spike, and common Pb; up to 1.0 pg of common Pb was assumed to be procedural blank:  $^{206}\text{Pb}/^{204}\text{Pb} = 18.50 \pm 1.0\%$ ;  $^{207}\text{Pb}/^{204}\text{Pb} = 15.50 \pm 1.0\%$ ;  $^{208}\text{Pb}/^{204}\text{Pb} = 38.40 \pm 1.0\%$  (all uncertainties 1-sigma). Excess over blank was assigned to initial common Pb, using the Stacey and Kramers (1975) two-stage Pb isotope evolution model at 104 Ma.  
 (f) Errors are 2-sigma, propagated using the algorithms of Schmitz and Schoene (2007) and Crowley et al. (2007).  
 (g) Calculations are based on the decay constants of Jaffey et al. (1971).  $^{206}\text{Pb}/^{238}\text{U}$  and  $^{207}\text{Pb}/^{206}\text{Pb}$  ages corrected for initial disequilibrium in  $^{230}\text{Th}/^{238}\text{U}$  using  $\text{Th}/\text{U}$  [magma] = 3.  
 (h) Corrected for fractionation, spike, and blank Pb only.  
 (i) Nominal fraction weights estimated from photomicrographic grain dimensions, adjusted for partial dissolution during chemical abrasion.  
 (j) Nominal U and total Pb concentrations subject to uncertainty in photomicrographic estimation of weight and partial dissolution during chemical abrasion.

**Table 5. U-Th-Pb isotopic data for sample MMI13-29-7.**

Compositional Parameters										Radiogenic Isotope Ratios						Isotopic Ages							
Wt.	U	Pb	Th	$^{206}\text{Pb}^*$	mol %	Pb*	Pb <sub>c</sub>	$^{206}\text{Pb}$	$^{207}\text{Pb}$	$^{206}\text{Pb}/^{207}\text{Pb}$	$^{206}\text{Pb}$	$^{235}\text{U}$	% err	$^{238}\text{U}$	% err	corr.	$^{207}\text{Pb}$	$^{206}\text{Pb}$	$^{206}\text{Pb}$				
mg	ppm	ppm	ppm	$\times 10^{-13}$	mol	Pb <sub>c</sub>	(pg)	$^{204}\text{Pb}$	$^{206}\text{Pb}$	$^{206}\text{Pb}$	$^{206}\text{Pb}$	$^{235}\text{U}$	% err	$^{238}\text{U}$	% err	coef.	$^{235}\text{U}$	$^{238}\text{U}$	$^{238}\text{U}$				
(a)	(j)	(i)	(b)	(c)	(c)	(c)	(c)	(d)	(e)	(e)	(e)	(f)	(f)	(e)	(f)	(f)	(g)	(f)	(g)	(f)			
<b>MMI13-29-7</b>																							
A	0.001	1291	47.9	0.814	1.3746	98.93%	31	1.20	1733	0.258	0.050017	0.910	0.220188	0.956	0.031928	0.141	0.396	195.77	21.14	202.07	1.75	202.61	0.28
B	0.001	252	9.2	0.743	0.4670	98.69%	24	0.51	1408	0.235	0.049784	1.545	0.218264	1.651	0.031797	0.159	0.691	184.93	35.97	200.46	3.00	201.79	0.32
C	0.001	741	12.3	0.415	0.3304	97.88%	14	0.59	873	0.133	0.048040	1.627	0.101294	1.736	0.015292	0.168	0.672	101.24	38.47	97.97	1.62	97.84	0.16
D	0.000	657	12.6	0.444	0.1326	95.25%	6	0.54	390	0.140	0.047577	6.321	0.105971	6.706	0.016154	0.447	0.871	78.31	150.07	102.27	6.52	103.30	0.46
E	0.000	1175	45.0	0.833	0.3102	97.79%	15	0.58	839	0.266	0.050372	0.889	0.219953	0.970	0.031669	0.190	0.506	212.21	20.61	201.87	1.78	200.99	0.37

(a) A, B etc. are labels for fractions composed of single zircon grains or fragments; all fractions annealed and chemically abraded after Mattinson (2005) and Scoates and Friedman (2008).

(b) Model Th/U ratio calculated from radiogenic  $^{208}\text{Pb}/^{206}\text{Pb}$  ratio and  $^{207}\text{Pb}/^{235}\text{U}$  age.

(c) Pb\* and Pb<sub>c</sub> represent radiogenic and common Pb, respectively; mol %  $^{206}\text{Pb}^*$  with respect to radiogenic, blank and initial common Pb.

(d) Measured ratio corrected for spike and fractionation only. Mass discrimination of 0.25‰/amu based on analysis of NBS-982; all Daly analyses.

(e) Corrected for fractionation, spike, and common Pb; up to 1.2 pg of common Pb was all assumed to be procedural blank:  $^{206}\text{Pb}/^{204}\text{Pb} = 18.50 \pm 1.0\%$ ;  $^{207}\text{Pb}/^{204}\text{Pb} = 15.50 \pm 1.0\%$ ;

$^{208}\text{Pb}/^{204}\text{Pb} = 38.40 \pm 1.0\%$  (all uncertainties 1-sigma).

(f) Errors are 2-sigma, propagated using the algorithms of Schmitz and Schoene (2007) and Crowley et al. (2007).

(g) Calculations are based on the decay constants of Jaffey et al. (1971).  $^{206}\text{Pb}/^{238}\text{U}$  and  $^{207}\text{Pb}/^{206}\text{Pb}$  ages corrected for initial disequilibrium in  $^{230}\text{Th}/^{238}\text{U}$  using  $\text{Th}/\text{U}$  [magma] = 3.

(h) Corrected for fractionation, spike, and blank Pb only.

(i) Nominal fraction weights estimated from photomicrographic grain dimensions, adjusted for partial dissolution during chemical abrasion.

(j) Nominal U and total Pb concentrations subject to uncertainty in photomicrographic estimation of weight and partial dissolution during chemical abrasion.

**Table 6. U-Th-Pb isotopic data for sample MMI13-4-8.**

Compositional Parameters										Radiogenic Isotope Ratios						Isotopic Ages							
Wt.	U	Pb	Th	$^{206}\text{Pb}^*$	mol %	Pb*	Pb <sub>c</sub>	$^{206}\text{Pb}$	$^{207}\text{Pb}$	$^{206}\text{Pb}/^{207}\text{Pb}$	$^{206}\text{Pb}$	$^{235}\text{U}$	% err	$^{238}\text{U}$	% err	corr.	$^{207}\text{Pb}$	$^{206}\text{Pb}$	$^{206}\text{Pb}$				
mg	ppm	ppm	ppm	$\times 10^{-13}$	mol	Pb <sub>c</sub>	(pg)	$^{204}\text{Pb}$	$^{206}\text{Pb}$	$^{206}\text{Pb}$	$^{206}\text{Pb}$	$^{235}\text{U}$	% err	$^{238}\text{U}$	% err	coef.	$^{235}\text{U}$	$^{238}\text{U}$	$^{238}\text{U}$				
(a)	(j)	(i)	(b)	(c)	(c)	(c)	(c)	(d)	(e)	(e)	(e)	(f)	(f)	(e)	(f)	(f)	(g)	(f)	(g)	(f)			
<b>MMI13-4-8</b>																							
A	0.0190	48	1.3	0.566	0.9530	99.68%	96	0.25	5801	0.180	0.049214	0.163	0.171247	0.234	0.025237	0.130	0.738	158.05	3.82	160.50	0.35	160.67	0.21
B	0.0052	224	6.1	0.458	1.2500	99.15%	36	0.86	2181	0.145	0.049192	0.413	0.174538	0.473	0.025733	0.157	0.524	157.00	9.67	163.35	0.71	163.79	0.25
C	0.0032	338	9.1	0.424	1.1561	99.20%	37	0.76	2322	0.135	0.049234	0.395	0.174107	0.456	0.025648	0.154	0.540	159.01	9.25	162.98	0.69	163.25	0.25
D	0.0045	313	8.4	0.456	1.5045	99.36%	47	0.79	2886	0.145	0.049269	0.299	0.174317	0.360	0.025660	0.144	0.588	160.66	6.99	163.16	0.54	163.33	0.23
E	0.0032	165	4.5	0.509	0.5628	98.91%	28	0.49	1701	0.161	0.048968	1.321	0.172604	1.407	0.025565	0.144	0.636	146.30	30.96	161.68	2.10	162.73	0.23

(a) A, B etc. are labels for fractions composed of single zircon grains or fragments; all fractions annealed and chemically abraded after Mattinson (2005) and Scoates and Friedman (2008).

(b) Model Th/U ratio calculated from radiogenic  $^{208}\text{Pb}/^{206}\text{Pb}$  ratio and  $^{207}\text{Pb}/^{235}\text{U}$  age.

(c) Pb\* and Pb<sub>c</sub> represent radiogenic and common Pb, respectively; mol %  $^{206}\text{Pb}^*$  with respect to radiogenic, blank and initial common Pb.

(d) Measured ratio corrected for spike and fractionation only. Mass discrimination of 0.25‰/amu based on analysis of NBS-982; all Daly analyses.

(e) Corrected for fractionation, spike, and common Pb; up to 0.9 pg of common Pb was all assumed to be procedural blank:  $^{206}\text{Pb}/^{204}\text{Pb} = 18.50 \pm 1.0\%$ ;

$^{208}\text{Pb}/^{204}\text{Pb} = 38.40 \pm 1.0\%$  (all uncertainties 1-sigma).

(f) Errors are 2-sigma, propagated using the algorithms of Schmitz and Schoene (2007) and Crowley et al. (2007).

(g) Calculations are based on the decay constants of Jaffey et al. (1971).  $^{206}\text{Pb}/^{238}\text{U}$  and  $^{207}\text{Pb}/^{206}\text{Pb}$  ages corrected for initial disequilibrium in  $^{230}\text{Th}/^{238}\text{U}$  using  $\text{Th}/\text{U}$  [magma] = 3.

(h) Corrected for fractionation, spike, and blank Pb only.

(i) Nominal fraction weights estimated from photomicrographic grain dimensions, adjusted for partial dissolution during chemical abrasion.

(j) Nominal U and total Pb concentrations subject to uncertainty in photomicrographic estimation of weight and partial dissolution during chemical abrasion.

**Table 7.** Laser ablation analysis results for sample 12JLO51-4.

<b>Age estimates with 1 sigma uncertainty (Ma)</b>						
<b>Analysis No.</b>	<b><math>^{207}\text{Pb}/^{235}\text{U}</math></b>		<b><math>^{206}\text{Pb}/^{238}\text{U}</math></b>		<b><math>^{207}\text{Pb}/^{206}\text{Pb}</math></b>	
	<b>Ma</b>	<b><math>\pm 1\sigma</math> Error</b>	<b>Ma</b>	<b><math>\pm 1\sigma</math> Error</b>	<b>Ma</b>	<b><math>\pm 1\sigma</math> Error</b>
PL1	338.7	5.49	337.4	2.62	334.3	40.78
12JLO51-4	223.3	5.48	221.5	2.19	284	59.18
2	220.3	15	220.2	4.95	232.8	155.74
3	219.3	22.42	222.2	6.18	203.2	233.62
4	223	6.6	224.1	2.54	251.3	70.16
5	215.8	12.54	212.4	4.09	374.3	132.62
6	221.7	8.65	218.6	2.9	228.2	92.3
7	219.3	13.9	218.7	4.72	152.7	145.64
8	229.2	9.7	222.3	3.21	298.3	98.9
9	217.2	13.73	217.2	4.55	243.7	145.69
10	226.7	12.22	216.8	3.8	272	124.97
11	208.1	11.23	208	3.78	301.5	124.39
12	229.7	6.48	228.9	2.58	228.3	66.6
13	227.3	13.32	224	4.78	388	128.95
14	225.8	20.58	221.5	6.96	291.7	199.81
15	231.2	11.49	230.6	4.2	225.2	112.9
16	241.9	14.58	233.6	5.26	473	131.21
17	229.6	11.65	226.8	4.13	217	115.93
18	225.3	11.39	222	4.02	243.7	115.46
19	225.4	13.82	224	4.59	259.3	139.47
20	225.8	15.62	226.9	5.56	147.4	156.54
21	231.7	14.89	227.4	5.26	420.7	141.07
22	215	11.68	215.9	4.04	300.8	123.41
23	208.6	9.08	210.6	3.47	192.2	99.75
24						

**Table 8.** U-Th-Pb isotopic data by laser ablation for sample MMI13-16-3.

<b>Grain Number</b>	<b><math>^{207}\text{Pb}/^{235}\text{U}</math></b>		<b><math>^{206}\text{Pb}/^{238}\text{U}</math></b>		<b>CE *vs**</b>	<b><math>^{206}\text{Pb}/^{238}\text{U}</math></b>		<b><math>^{207}\text{Pb}/^{206}\text{Pb}</math></b>		<b><math>^{207}\text{Pb}/^{235}\text{U}</math></b>	
	<b><math>\pm 2\sigma^*</math></b>		<b><math>\pm 2\sigma^{**}</math></b>			<b><math>\pm 2\sigma</math></b>		<b><math>\pm 2\sigma</math></b>		<b><math>\pm 2\sigma</math></b>	
MMI13_16_3_1	0.212	0.020	0.03297	0.0016	0.079557	208.9	9.8	0.0491	0.004	197	16.0
MMI13_16_3_2	0.239	0.020	0.03313	0.0015	0.17834	209.9	9.3	0.0529	0.004	214.8	16.0
MMI13_16_3_3	0.225	0.019	0.0328	0.0015	0.28517	207.9	9.4	0.0495	0.004	202.9	16.0
MMI13_16_3_4	0.2276	0.017	0.03268	0.0014	0.21927	207.5	8.7	0.0507	0.003	208	14.0
MMI13_16_3_5	0.233	0.017	0.03324	0.0014	0.56452	210.7	8.8	0.0512	0.003	212.5	14.0
MMI13_16_3_6	0.2182	0.018	0.03195	0.0014	0.30674	202.6	8.9	0.0501	0.003	199.2	15.0
MMI13_16_3_7	0.2383	0.017	0.03421	0.0015	0.65598	216.7	9.3	0.05133	0.003	217.8	14.0
MMI13_16_3_8	0.2277	0.017	0.03361	0.0015	0.39965	213	9.3	0.0495	0.003	208.5	14.0
MMI13_16_3_9	0.2389	0.017	0.03429	0.0014	0.37134	217.5	9.0	0.0507	0.003	216.9	14.0
MMI13_16_3_10	0.2284	0.018	0.03286	0.0015	0.18967	208.3	9.5	0.0504	0.003	209.4	15.0
MMI13_16_3_11	0.2138	0.016	0.03191	0.0014	0.36845	202.4	8.7	0.0489	0.003	196.6	13.0
MMI13_16_3_12	0.2359	0.018	0.03477	0.0018	0.72474	220.2	11.0	0.0484	0.003	215	14.0
MMI13_16_3_13	0.224	0.017	0.0331	0.0015	0.66294	209.8	9.6	0.0489	0.003	205.6	14.0
MMI13_16_3_14	0.224	0.018	0.03358	0.0016	0.33965	212.8	9.7	0.0486	0.003	205.9	15.0
MMI13_16_3_15	0.2199	0.017	0.03286	0.0014	0.34091	208.3	8.9	0.0478	0.003	202.2	14.0
MMI13_16_3_16	0.25	0.025	0.034	0.0017	0.30709	215.3	11.0	0.0531	0.005	224	20.0
MMI13_16_3_17	0.2336	0.018	0.03401	0.0017	0.6308	215.5	11.0	0.0494	0.003	213.1	14.0
MMI13_16_3_18	0.225	0.019	0.03308	0.0015	0.35251	209.7	9.4	0.0486	0.003	205.6	15.0
MMI13_16_3_19	0.239	0.030	0.0359	0.0022	0.096084	227	13.0	0.0522	0.007	214	24.0
MMI13_16_3_20	0.232	0.019	0.03292	0.0015	0.12325	208.7	9.5	0.0516	0.003	211.9	15.0

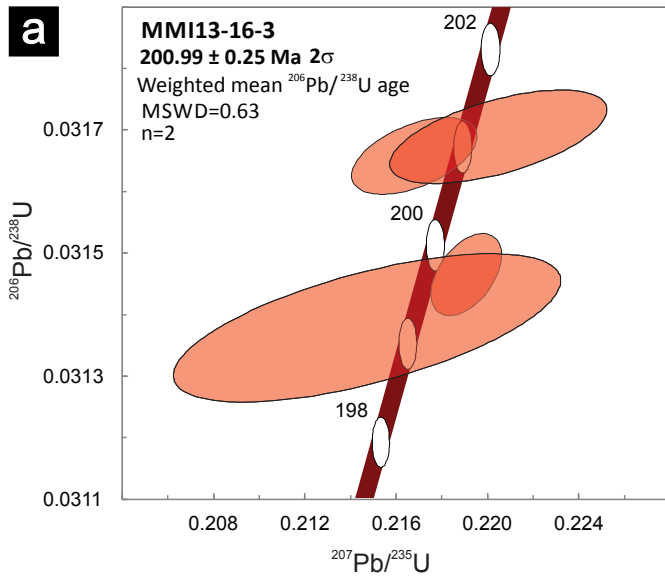


**Fig. 18. a)** Thermal Ionization Mass Spectrometric (TIMS) analysis of zircon U-Pb from sample MMI13-16-3 of dike in b) yields an age of  $202 \pm 4$  Ma based on two overlapping fractions on concordia. Slightly younger grains are discordant. Data point error ellipses are  $2\sigma$ . **b)** Near-vertical, fine-grained dike cuts maroon and green volcanic sandstone and granule conglomerate (black arrow marks southeast contact).

swarm was previously mapped as part of the Bromley pluton, but the lithologic character and dike orientation more closely resemble those of the ‘Mine dikes’, well exposed to the south, and dated at  $102.9 \pm 0.3$  Ma at the Copper Mountain mine (Mihalynuk et al., 2010). To confirm this reassignment, we collected a sample for age determination. Analysis of 5 grains extracted show that they mutually overlap concordia at  $103.9 \pm 0.2$  Ma with no hints of inheritance (Fig. 20b), and are most likely genetically related to the Mine dike swarm.

#### 9.4.5. Southwest Zone, Miner Mountain: Sample MMI13-29-7

Following previous unsuccessful attempts at U-Pb dating of

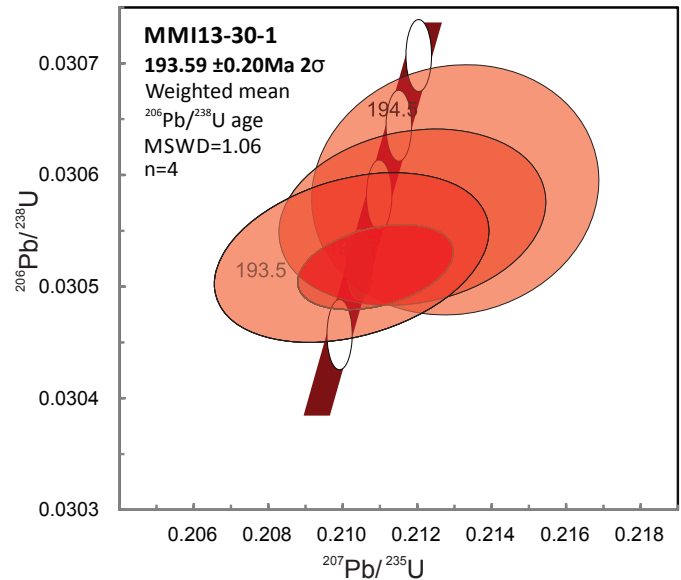


**Fig. 19.** Thermal Ionization Mass Spectrometric (TIMS) analysis of zircon U-Pb from sample MMI13-30-1 of pegmatitic dikes west of the Bromley pluton. An age of  $193.6 \pm 0.3$  Ma is based on four overlapping fractions on concordia.

intrusions at Miner Mountain due to zircon poor-lithologies, we processed two boxes of core from the Southwest Zone that had been sawn in half (drillhole DDH13, 3.45 m to 11.11 m). Only 7 zircon grains were recovered (five were faceted and 2 subrounded, Fig. 21a), five of these survived chemical abrasion pre-treatment and were analysed (Fig 21b; Table 5). They yielded a broadly bimodal spread of results: three overlap concordia at ca. 200-203 Ma ( $\text{Th}/\text{U} = 0.74\text{-}0.83$ ), and two at ca. 98-103 Ma ( $\text{Th}/\text{U} = 0.42\text{-}0.44$ ). The older population is interpreted as having inherited xenocrystic material and the younger as largely primary magmatic zircon that records the crystallization of this intrusion. The more subtle spread of ages within each of the two groupings may be due to minor Pb loss not mitigated through chemical abrasion pre-treatment, a physical mixture of populations (minor older cores in younger grains or younger rims on older grains), or a combination of the two. It is not possible with the current data to confidently choose between these possibilities, so we conservatively assign a crystallization age of  $\sim 100 \pm 3$  Ma for this rock, with  $\sim 200$  Ma inheritance.

#### 9.4.6. Osprey Lake batholith: Sample MMI13-4-8

Sample MMI13-4-8 (Table 6; Fig. 22) is from grey-weathering, porphyritic granodiorite that cuts and thermally metamorphosed flow-banded rhyolite and andesite breccia in the headwaters of Swanson Creek. Mihalynuk and Logan (2014a) mapped the volcanic package as Early Cretaceous because of strong similarity and continuity with the suite of rocks farther west (e.g. Monger, 1989) and interpreted the porphyritic intrusion as belonging to the younger Summers Creek suite of intrusions, which has returned K-Ar cooling ages of  $\sim 98$  Ma (Preto, 1979; recalculated in Breitsprecher

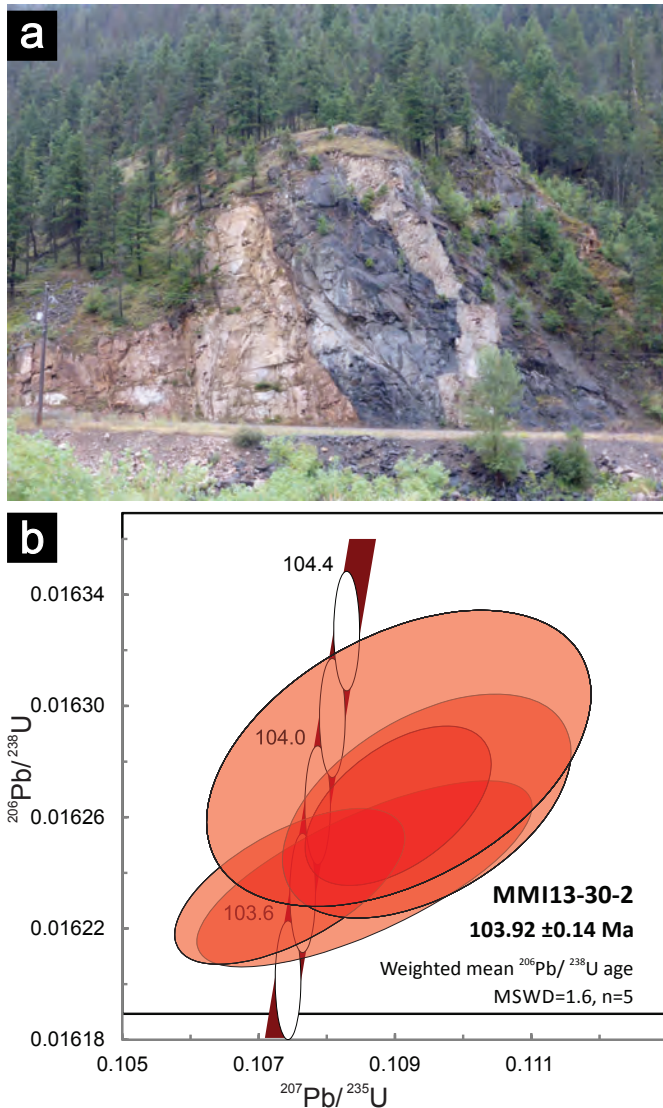


**Fig. 20. a)** View to south, across the Similkameen River; north-trending 'Mine dikes' (pink) cut dark green volcanosedimentary Nicola Group country rocks. **b)** Concordia plot shows cluster of 5 grains analyzed from 'Mine dike' sample MMI13 30-2 at  $103.9 \pm 0.2$  Ma.

and Mortensen, 2005). However, zircons extracted from the intrusion overlap concordia between 160 Ma and 164 Ma (Fig. 22a) requiring the volcanic package to be Late Jurassic or older. To ensure that the TIMS ages were not erroneously old as a consequence of older xenocrystic cores, 11 grains were examined by cathodoluminescence (Fig. 22b) and the rims and cores of 10 grains were analyzed by laser ablation (LA-ICPMS). Neither cathodoluminescence, nor laser dating revealed any evidence of cores or strong overgrowths. Rather, these analyses confirm the TIMS ages with a weighted age for 9 of the 10 zircons at  $162 \pm 2$  Ma (range from 156–167 Ma  $\pm 5$  Ma for individual analyses; see Mihalynuk et al., 2015 for the complete dataset). One grain yielded a slightly younger age ( $\sim 145 \pm 5$  Ma); however there is no evidence of younger,  $\sim 100$  Ma rims on any of the zircons.

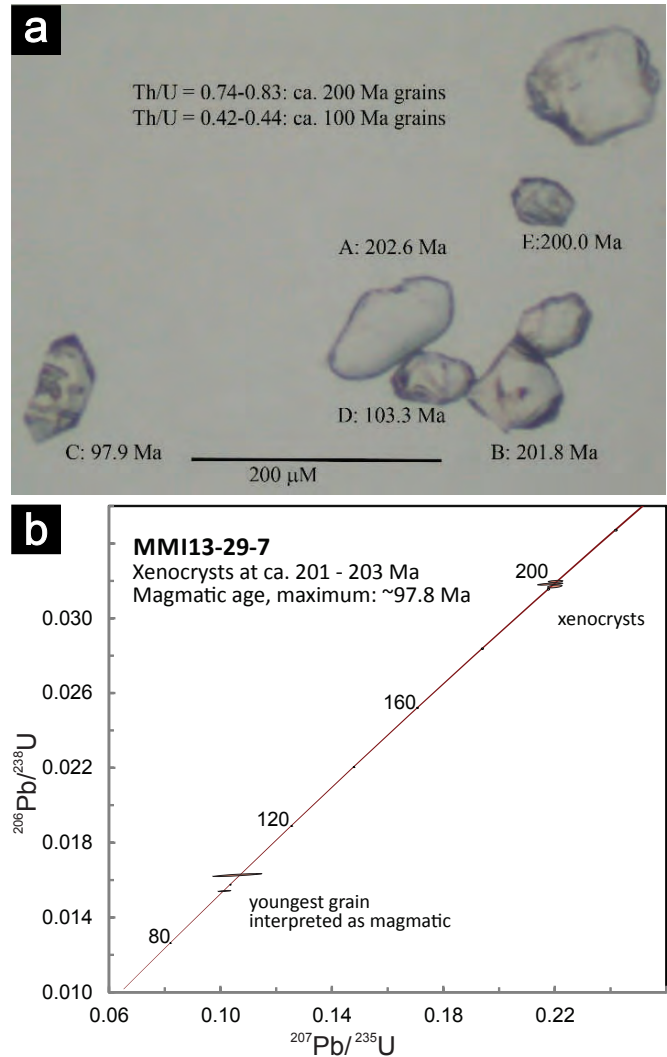


**Fig. 21. a)** Photomicrograph of zircons from sample MMI13-29-7 of drill core intersected by drilling at Miner Mountain, southwest zone prior to chemical abrasion. **b)** Thermal Ionization Mass Spectrometric (TIMS) analysis of zircon U-Pb. Multiple fractions lie on concordia. The age of this intrusion is most likely  $\sim 98$  Ma; it contains  $\sim 200$  Ma xenocrystic zircons.

We have collected the rhyolite with the aim of confirming a previously unrecognized older felsic volcanic package in the Swanson Creek area as required by the age data. A corollary is that the porphyritic intrusion is part of the huge Osprey Lake batholith with a U-Pb crystallization age of  $166 \pm 1$  Ma (Parrish and Monger, 1992). Analyses are pending.

#### 9.4.7. Detrital zircon analysis of Voght unit sandstone: Samples JLO12-51-4 and MMI13-16-5

Two samples of maroon sandstone (Tables 7 and 8; Fig. 23) interpreted to bracket deposition of the Voght unit, were collected from sites along the Coquihalla Highway that are separated by  $\sim 9$  km. The samples were submitted for detrital zircon analysis by LA-ICPMS to determine maximum depositional ages as given by the youngest zircon. In active

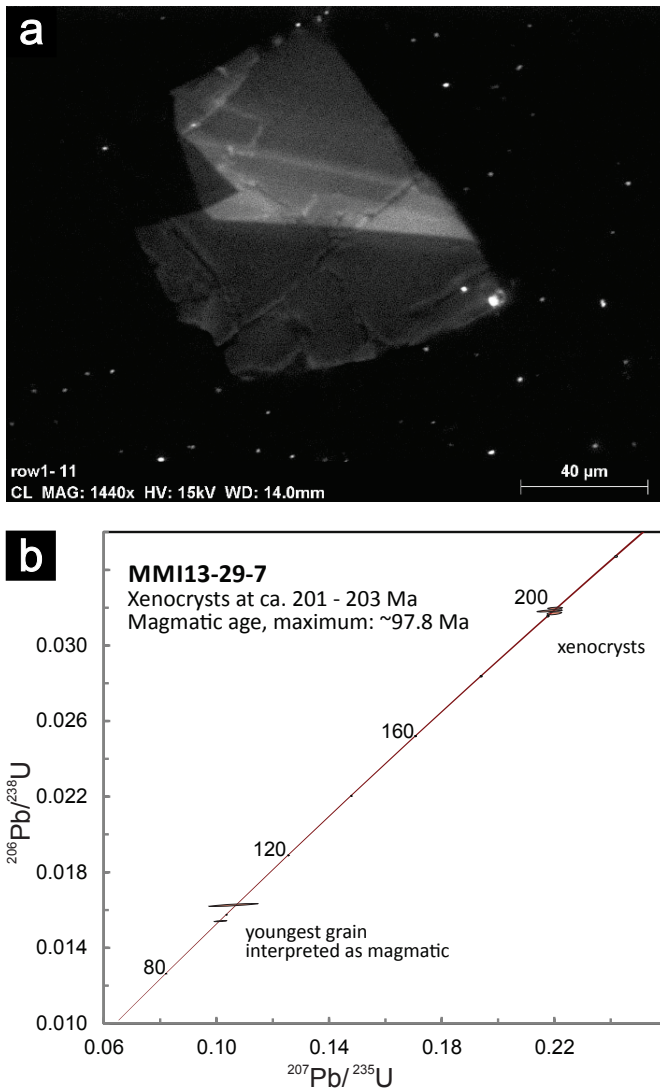


**Fig. 22.** **a)** Concordia plot for sample MMI13-4-8 of porphyritic granodiorite. **b)** Cathodoluminescent image of a zircon extracted for follow-up LA-ICPMS dating. Growth bands are visible, but evidence of overgrowths or a xenocrystic core are lacking.

volcanic terranes, the age of the youngest detrital zircons commonly closely corresponds to the actual depositional age, given the error of the analytical technique and time scale uncertainties (e.g. Evenchick et al., 2010).

Twenty zircons were analyzed from each sample and the age of youngest zircons date the Voght unit between  $208 \pm 4$  Ma (Fig. 23a) and  $202 \pm 4$  Ma (Fig. 23b). Including  $1\sigma$  errors, this age spans most of the late Norian (Late Triassic) through to the Hettangian (earliest Jurassic, IUGS timescale, Cohen et al., 2013). However, the younger age is further constrained as being older than  $201 +0.3/-0.4$ Ma, based on the TIMS age determination of the cross-cutting dike (sample MMI13-16-5; Fig. 18a, see above), making the entire Voght section Late Triassic. Pillow breccia intercalated with the inferred older part of the succession, is probably of Middle Norian age (~208 Ma).

## 10. Structure

Evidence for contractional deformation can be found at all scales in layered rocks of the Shrimpton map area. However, the lack of continuous exposures means that large-scale structures must be inferred from regional strike and dip information combined with outcrop distribution patterns. For example, a faulted, open, north-northeast-trending, mountain-scale anticlinal hinge that occupies the Kane Valley has been defined by tracing out a previously unmapped carbonate unit. This anticline parallels the general structural grain in the region (Fig. 3).

Observations of outcrop-scale folds are mostly limited to new exposures, mainly roadcuts. Massive bedrock incisions along the Coquihalla Connector (Highway 97C) are especially instructive because the highway cuts across strike. For example, west of the Loon Lake turnoff are excellent new exposures of folded strata and near-bedding parallel fault zones interpreted as thrust faults (Fig. 24a). Most thrusts appear to cut up section to the east. An exception to east-directed thrust faults are those interpreted to carry Triassic strata westward over the Bates unit. Because most thrust faults cannot be traced along strike, amounts of shortening across them are unconstrained.

Ductile fabrics are developed in the thermal metamorphic halo around the Early Jurassic Pennask batholith, but are lacking, except within tens of m of the contact around the even more extensive Osprey batholith. For example, within about 1km of the Pennask contact, incipient chlorite-actinolite schistosity is developed in the Boot Lake unit of the Paradise succession, along with discrete dextral and sinistral shear zones (Fig. 24b).

Most ocean lithosphere subduction beneath volcanic arcs today is non-orthogonal. Such oblique subduction results in strain partitioning: the normal component causes shortening concentrated in the accretionary complex and forearc, and the arc-parallel component causes transverse faulting concentrated along the hot, weak, arc axis (McCaffrey et al., 2000). Shortening in the Nicola arc accretionary complex is recorded by Cache Creek Group rocks exposed well to the west of the map area (Savona to Cache Creek; Monger and McMillan, 1989). Transverse faulting expected along the arc axis is probably recorded by the Summers and Allison creeks faults; possibly long-lived, steep fault systems that have long been recognized (Preto, 1979, Monger, 1989, and others). This >160km-long fault system is suspected to have focused emplacement of mineralized Late Triassic plutons (Preto, 1979). However, the question of the amount of offset has not been addressed.

Distinctive biotite-quartz-apatite-phyrific volcanic units of the Zig unit, and clastic rocks derived from it, have not been recognized south of the Shrimpton area (e.g. Preto, 1979; Mihalynuk et al., 2014), nor are we aware of the unit having been mapped to the north (e.g. Preto, 1967, 1979; Kwong, 1987; Logan and Mihalynuk, 2005a, b). Assuming that these workers have not overlooked the distinctive rock units, it would appear that the units do not extend tens to hundreds

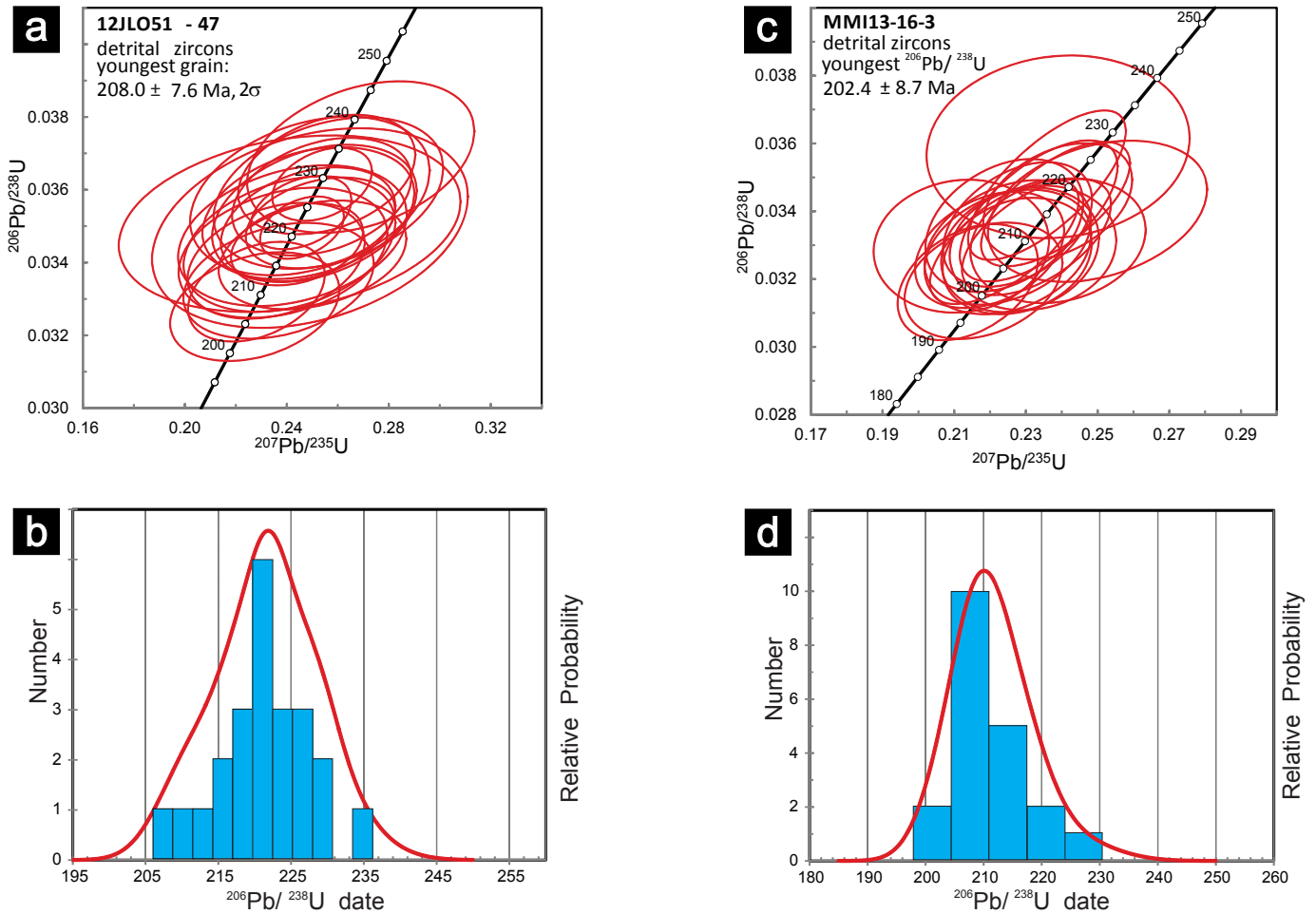


**Fig. 23.** a) Concordia plot and b) histogram of detrital zircon ages from the approximate base of the Voght unit maroon volcanic sandstone. c) Concordia plot and d) histogram of detrital zircon ages from the upper Voght unit. Both samples are Late Triassic (229-201 Ma; Cohen et al., 2013).

of kilometres along the arc. Rather, the Zig unit and derived clastic rocks may be restricted to the Shrimpton area on both sides of northern strands of the Summers Creek Fault, known as the Kentucky-Alleyne Fault through much of the Shrimpton Creek map area. This is an important observation, because if accurate, it severely limits offset on the fault. Although offset on Summers Creek Fault was apparently insufficient to displace the Zig unit and derived clastic units, offset prior to Zig unit deposition is unconstrained. Kentucky-Alleyne Fault strands must swing west of the Pennask batholith, as is shown by Preto (1979), because the trace of the batholith's southern contact can now be extended almost as far west as Pothole Lake (Fig. 3).

At the southern border of the Shrimpton map area, the Allison Creek Fault cuts the Allison pluton, appears to juxtapose Spences Bridge Group with the intrusion, and may have been active during deposition of the Cretaceous volcanic succession, as discussed by Mihalynuk et al. (2014a). Amounts of Late Triassic and younger offset on the Allison Creek fault are limited by the amount of apparent offset of the Allison pluton. Because the pluton is elongated subparallel to the fault (Fig. 3) and intrusive contacts with country rocks are largely obscured

by cover, the amount of apparent lateral offset along the Allison Creek fault cannot be estimated with certainty. However, it is probably less than 10 km.

## 11. Mineralization

More than 100 years of active exploration in the Shrimpton area has resulted in discovery of more than 130 MINFILE occurrences. One of the first showings to be explored in the Aspen Grove Copper Camp was the Big Sioux. It was staked in 1899, developed by underground workings and produced hand-sorted ore containing copper minerals that included chalcopyrite, bornite, malachite, chalcocite and cuprite. Historical mineral production since those early days reportedly came from three mineral deposit types; placer gold (Shrimpton Creek, MINFILE 092HNE180 and Siwash Creek, MINFILE 092HNE290), Au-quartz veins (Elk, (Siwash Mine) MINFILE 092HNE096) and alkalic porphyry Cu-Au-Ag (Big Sioux, MINFILE 092HNE073 and Copper Star, 092HNE036).

Major exploration and development programs were completed by three mining companies in the Shrimpton area in 2014. Bulk sample mining, begun in 2013 by Gold Mountain



**Fig. 24.** a) Folding and thrust faulting of Shrimpton succession wacke unit west of the Loon Lake turnoff, Coquihalla Highway. Thrust fault (red dotted line) juxtaposes near-vertical beds in footwall against subhorizontal beds in hanging wall. b) Incipient foliation in hornblende-pyroxene conglomerate of the Boot Lake unit.

Mining Corp. at their Elk Project (Siwash Mine), was completed this fall with shipment of 6668 tonnes of mineralized material expected to yield an average grade of 17.3 g/t Au (Gold

Mountain Mining Corporation, 2014). The Au-Ag mineralized pyritic quartz veins are thought to be Tertiary and related to Otter intrusions (Pooley et al., 2011). Fjordland Exploration Inc. completed a preliminary soil sampling and 2070 m surface trenching program (East Dillard) followed by a 14-hole, 5,574 m diamond drill program on both Dillard East and Dillard West porphyry copper-gold targets, approximately 15 km southwest of the Elk Project. Kaizen Discovery Inc. carried out a diamond drilling program at their Par prospect (described below), following-up on the results of a 2013 geological mapping and sampling program completed by West Cirque Resources Ltd. (Kaizen Discovery Inc., 2014).

We limit our discussion below primarily to undocumented, possibly new, occurrences and to existing MINFILE occurrences with new observations or geochemical analyses (Table 9) to report.

#### 11.1. Par prospect (MINFILE 092HNE169)

Kaizen Discovery Inc. completed 2,012 metres of diamond drilling in four holes that tested 880 metres of potential VMS mineralized strike length on their Par prospect, in

**Table 9.** ICP-MS analytical results for select samples and elements.

StatNum	Type	UTM E	UTM N	Ag	As	Au	Ba	Bi	Co	Cs	Cu	Fe	Hg	In	Mn	Mo	Ni	Pb	Re	S	Sb	Se	Te	Zn
				ppb	ppm	ppb	ppm	ppm	ppm	ppm	ppm	%	ppb	ppm	ppm	ppm	ppm	ppm	ppb	%	ppm	ppm	ppm	ppm
GMc14-05-13	1.3m chip	687575	5513992	387	5.9	54.8	33	0.23	13.8	2.76	287.33	4.95	<5	<0.02	116	2.09	23	2.52	8	2.7	0.39	1.8	1.05	18.1
GMc14-05-13b	20cm chip	687575	5513992	450	44.7	23.6	93.6	0.16	10.3	8.01	136.75	3.81	120	0.05	938	1.27	21	3.39	7	1.25	3.37	0.7	0.51	29.2
GMc14-61-3	Assay grab	670558	5502382	303	4.8	73.8	26.6	1.57	20.9	0.19	178.14	3.71	<5	0.04	216	0.27	36	1.88	1	2.65	0.14	0.4	0.94	26.3
MM14-02-6	3m chip	672712	5532632	3767	37.7	3.6	46.1	0.37	23.8	0.3	>10000.00	3.12	121	<0.02	756	0.95	12	1.11	2	0.07	0.65	0.9	0.29	55.2
MM14-09-7	Assay grab	681991	5524340	269	2.1	1.3	153.5	0.16	17.7	2.48	153.91	3.26	<5	0.03	978	1.15	26	2.82	2	0.24	0.39	1.6	0.03	50.2
MM14-18-4	chip	682905	5558331	68084	27.3	322.8	17.8	0.48	10.8	0.18	>10000.00	6.53	73	0.11	684	117.1	11	35.29	<1	0.27	1.11	8.8	7.12	106.9
MM14-19-6	Assay grab	685541	5517303	282	0.8	122.2	37.6	0.04	12.8	1.63	466.75	3.09	16	<0.02	446	0.11	5.6	0.59	<1	<0.02	<0.02	<0.1	0.08	40
MM14-24-12	Assay grab	676868	5516880	1209	21.6	170.1	547.4	0.05	24.6	0.18	4765.58	5.67	15	<0.02	1476	0.84	5.3	15.91	<1	0.03	0.1	1.8	<0.02	161.2
MM14-39-1	Assay grab	678706	5521179	53	3.5	1.8	14.9	<0.02	8	0.41	252.91	2.13	34	<0.02	659	0.21	3.4	1.93	<1	0.06	0.24	<0.1	0.05	34.2
MM14-41-07	Assay grab	676505	5525203	250	19.9	3.3	84.9	0.14	17.1	1.48	3294.72	4.19	8	0.03	1106	0.47	8.9	2.7	<1	<0.02	0.21	<0.1	<0.02	88.5
MM14-41-10	Assay grab	675935	5525883	112	7.8	4.5	23.5	0.03	7.5	0.07	12.69	2.87	107	<0.02	469	3.12	2.3	6.92	5	1.38	0.3	0.4	0.04	22
MM14-50-09b	Assay grab	666460	5507872	86078	15.5	5	4134.1	0.96	16.4	4.22	1758.81	2.61	628	<0.02	416	0.27	55	996.8	2	0.1	135.9	0.2	0.37	482.7
MM14-50-09c	Assay grab	666460	5507872	28464	2.3	4.4	5399.3	0.26	10	3.89	541.77	1.99	151	<0.02	229	0.46	28	194	<1	0.09	19.65	<0.1	0.14	256.4
MM14-50-10	Assay grab	666492	5507891	255	4.9	2.8	60	0.04	80.4	18.11	51.27	6.36	<5	0.02	734	0.7	334	18.55	<1	<0.02	1.67	<0.1	0.03	301.9
MM14-50-11	Assay grab	666450	5507870	>100000	21.5	2	>10000.0	0.55	5	1.07	1900.27	1.01	430	0.02	223	0.82	20	4714	<1	0.06	217.9	0.2	0.61	194.6
MM14-52-07	Assay grab	666944	5505292	243	<0.1	0.5	313.1	0.05	1.4	0.06	17.05	1.52	<5	<0.02	68	10.02	1.1	10.02	22	0.22	0.59	0.4	0.06	8.8
MM14-54-02	Assay grab	692527	5516847	21564	16.6	75.2	15.8	4.58	10.3	0.58	1425.57	5.52	425	22.69	814	2.91	1.4	874	2	7.33	3.81	2.7	0.22	>10000.0
MM14-54-11	Assay grab	698019	5515139	2422	2.1	<0.2	30.5	0.18	11.7	0.4	62.47	3.6	14	0.03	8382	0.26	41	3257	<1	1.28	0.61	<0.1	0.1	3242.4
MM14-54-13a	Assay grab	698021	5515146	388	0.5	1.1	9.4	0.12	4	0.11	3.92	1.63	<5	<0.02	>10000	2.95	12	544.7	<1	0.93	0.17	<0.1	0.03	543.8
MM14-54-13b	Assay grab	698021	5515146	295	0.8	1.1	58.5	0.04	6.8	0.39	15.9	2.17	<5	<0.02	5530	19.2	7.6	130.5	2	0.76	0.31	<0.1	0.02	411.7
MM14-50-10	grab dup	666492	5507891	273	4.6	1.4	64.6	0.03	68.8	19.24	49.85	6.74	<5	<0.02	729	0.56	351	19.28	<1	<0.02	1.68	<0.1	<0.02	302.1
MM14-50-10	grab dup	666492	5507891	285	5.1	1.1	66.2	<0.02	74.1	19.09	48.67	7.13	<5	<0.02	782	0.63	376	19.17	<1	<0.02	1.64	<0.1	<0.02	312.1
<b>Detection Limit</b>				2	0.1	0.2	0.5	0.02	0.1	0.02	0.01	0.01	5	0.02	1	0.01	0.1	0.01	1	0.02	0.02	0.1	0.02	0.1

southeast Shrimpton Creek map area. The mineralization and alteration observed in core indicates at least two styles of mineralization; a hybrid high-level porphyry-high sulfidation epithermal system; and volcanogenic massive sulfides (Kaizen Discovery Inc., 2014). The alkalic porphyry/breccia type Cu-Au-Mo mineralization appears to be superimposed on the early synvolcanic mineralization. Mineralization includes massive to semi-massive intervals of copper, zinc, silver, gold and molybdenum-bearing sulphides. It is contained in broad intervals of intense silicification, and phyllic and advanced argillic alteration zones in high-level quartz-feldspar porphyry intrusions and related felsic volcanic and volcanoclastic rocks (Kaizen Discovery Inc., 2014).

### 11.2. Ketchan Lake North prospect (MINFILE 092HNE115)

The Ketchan Lake North porphyry Cu-Au-Ag-Pd±Pt prospect is in the southeast part of the Shrimpton Creek map area, where maroon pyroxene-olivine-analcite phyrlic volcanic rocks are intruded by a high-level, northwest-trending alkaline monzodiorite intrusion, (Ketchan Lake stock; Fig. 25). Pyroxene-biotite diorite and hornblende±pyroxene monzodiorite to monzonite are the main intrusive phases; mineralization is focused in the monzonite. Sub-circular breccia pipes with magnetite-healed breccias and elevated Cu and Au values intrude the intrusive complex. Analyses of two samples of Ketchan Lake mineralization were reported in Mihalynuk et al. (2014a). Sample JLO13-23-8 (Zone 10, NAD83; 676833 E, 5516535 N) is a brecciated hornblende monzonite healed by anastomosing K-spar and magnetite and overprinted by shallow, east-trending epidote fracture fillings and replacement zones. Sample JLO13-23-9 (Zone 10, NAD83; 676763 E, 5516564 N) is a pervasive K-spar and albite altered monzonite cut by mm to cm steep, north-trending veinlets of chalcopyrite±pyrite with pink K-spar vein selvages. Higher gold and silver values have a direct relationship to higher copper values. Analyses of Ketchan Lake mineralization also reveals some of the highest Pt (35 ppb) and Pd (323 ppb) values in the study area (Mihalynuk et al. 2014a, Table 1).

The Ketchan Lake stock is one of several alkalic intrusive centers in the Shrimpton map area, including Big Kidd (Fig. 2; MINFILE 092HNE074). All are undated but are presumed correlative with the alkalic Copper Mountain Intrusive Suite (<205 Ma) that hosts the Copper Mountain, New Afton and Mount Polley mines in southern British Columbia.

### 11.3. Snowstorm prospect (MINFILE 092HNE032)

The Snowstorm prospect, also known as the Siwash Creek property, is classified in MINFILE as a shear-related vein. However, little evidence of a major shear zone is present: mineralization occupies dilatant quartz-calcite-sphalerite-galena±chalcopyrite vein stockworks and is broadly related to strongly clay altered porphyritic 'Otter intrusion'. The base metal veins at the Snowstorm may have formed distal to a buried porphyry system, a model that has been partly tested by Cu and Mo geochemical surveys (Banks, 1980) and a regional

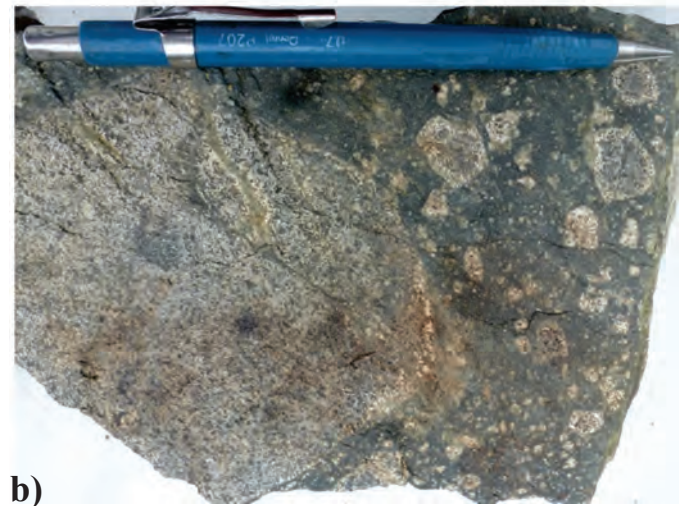
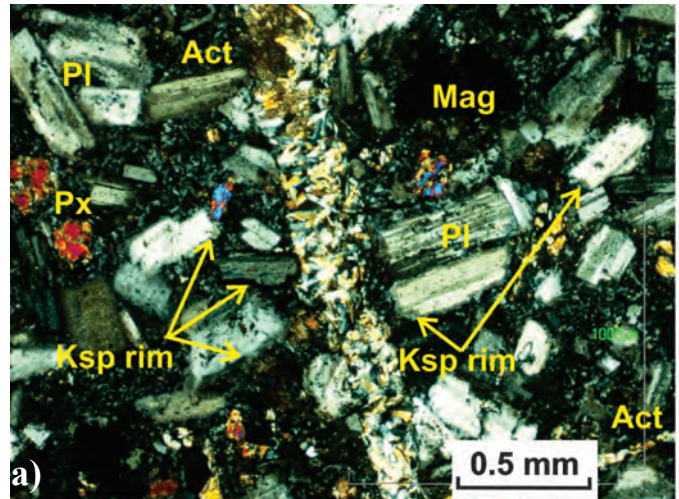


**Fig. 25. a)** Photomicrograph of Ketchan Lake stock. Pyroxene-hornblende and stubby plagioclase porphyritic monzodiorite flooded by secondary K-spar and cross-cut by actinolite and calcite (violets), cross polarized light. **b)** Chlorite+magnetite matrix supported monzodiorite intrusive breccia.

drilling campaign by Brenda Mines (Groves, 1989).

Old dumps, tracks and collapsed adits are relicts of underground mining dating to 1917, when most work entailed drifting along the veins. According to Groves (1989), 27 tons of ore shipped to Trail in 1927 yielded 3 oz. gold, 3,379 oz. silver, and 1,578 lbs of lead. We sampled well-mineralized vein material on surface from above the collapsed main adit (Fig. 3; sample MMI14-54-02). It contained element values consistent with the observed sulphide mineralogy: i.e. >10,000 ppm Zn, 874 ppm Pb, 21.6 ppm Ag, and significantly, 22.7 ppm In (Table 9). Indium does not form primary mineral deposits but elevated values commonly accompany sphalerite mineralization (Briskey, 2005).

#### 11.4. Margerri

Chocolate-coloured carbonate-cemented breccia of fine feldspar porphyry dikes and clay-altered, pyritic quartz-feldspar porphyry locally contains mm-thick veinlets of galena, sphalerite, and chalcopryite at the Margerri showing (Fig. 26a). Analysis of three mineralized samples range up to 0.32% Zn, 0.32% Pb and 2.4 ppm Ag. Alteration mineralogy and intrusive texture of the porphyry are similar to the host porphyry at the Snowstorm (Fig. 26b). Analysis of predominantly matrix material (Table 9, MMI14-54-13a) returned >1% Mn, 1.6% Fe and 2.83% Ca, suggesting that the matrix material comprises a brown weathering Mn-Fe oxide intergrown with calcite. Margerri is not catalogued in MINFILE, and there is no indication that it has been sampled previously; although any sample collection markings may have been removed because the breccia is in a small borrow pit, actively being used as road ballast. Approximately 100 m to the north, similar mineralization is exposed at a logging landing (Fig. 26c).

#### 11.5. DaBren

In the northwestern part of the Summers Creek map area, broken outcrops along the Pike Mountain logging road (Fig. 2; Mihalynuk et al., 2014a) include blocks of quartz  $\pm$  carbonate-barite veins up to 35 cm thick. Quartz contains outlines of bladed, 1 to 2 cm-long crystals interpreted to be silicified carbonate. Mineralization occurs as blebs and discontinuous veinlets of sphalerite and chalcopryite and dark grey, vein-parallel banding. Analysis of mineralized samples returned Pb and high Ag values, perhaps indicative of argentiferous galena (Table 9, MMI12-50-09b, c: up to 0.5% Ba, 0.17% Cu, 0.1% Pb, 0.04% Zn and 86 ppm Ag). Our samples returned only low Au contents (up to 5 ppb). This epithermal precious metal vein occurrence is not catalogued in MINFILE.

#### 11.6. Leeman

Rubbly, rust and copper-stained quartz vein scree occurs near the crest of a low glacial ridge in the grassland between Quilchena and the northeast corner of the Shrimpton map area (Fig. 2). Excavation of the vein revealed that it is up to 35 cm thick and has chalcopryite along banded margins and a cockscomb interior. Host rocks are tan, well-bedded cherty argillite and siltstone. A composite chip sample was taken across the vein from two sites separated by ~3 m. ICP-MS analysis (MMI14-18-4; Table 9) shows that the vein contains elevated Au (0.3 ppm), Ag (68 ppm), Cu (>1%) and Zn (0.01%). This precious and base metal-rich vein is not catalogued in MINFILE.

#### 12. Conclusions

Geological fieldwork between Princeton and Merritt in 2014 extended 2013 mapping in the Summers Creek area northward to the Shrimpton Creek area, covering NTS sheets 092H/15E and 16W. Field and laboratory results arising from this work have changed the way we perceive the Late Triassic arc and its overlying strata.

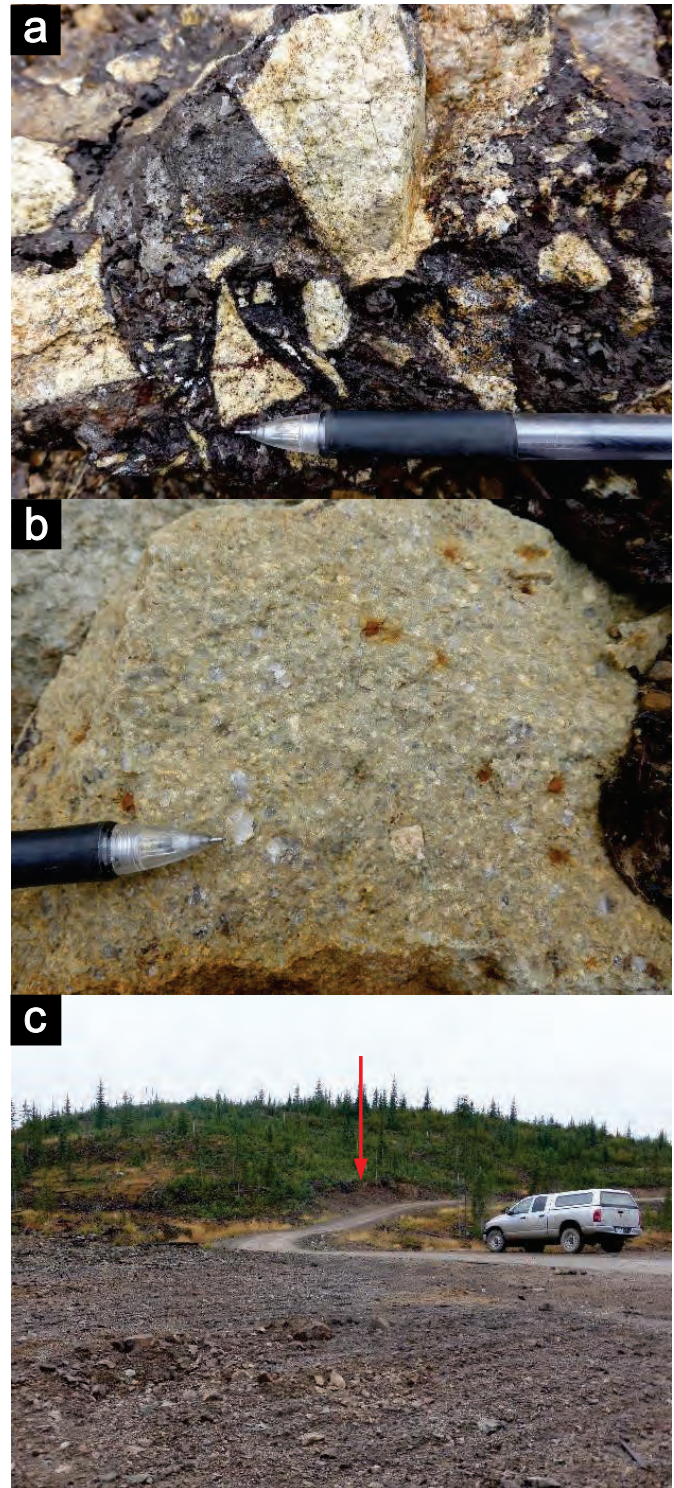


**Fig. 26.** a) Chocolate-coloured Mn-Fe oxide and carbonate interstitial to angular fragments of altered quartz-feldspar porphyry. b) Clay-altered quartz-feldspar porphyry is similar to host rocks at the Snowstorm prospect. c) Main mineralized breccia in borrow pit at Margerri is beyond the corner in the road (arrow) and similar mineralization is found as disturbed subcrop at the logging landing in the foreground.

Nicola arc strata are both older and younger than previously recognized. A new U-Pb crystallization age of ~238 Ma from a rhyolite tuff in the Central belt (Preto, 1979) is the oldest dated unit in the Nicola Group.

Felsic volcanism, previously thought to be characteristic of Preto's (1979) Western belt extends into the Central belt.

The 'Zig unit', a newly recognized distinctive biotite-quartz-apatite porphyry, and clastic rocks derived from it, span the Summers Creek fault, limiting significant motion on the fault to before ~210 Ma.

A marker succession recognized in the Kane Valley permits definition of a regional anticline.

Mainly eastward-vergent contractional deformation is recorded by thrust faults and folds that are well displayed in sedimentary successions.

Three base and precious metal vein occurrences not catalogued in MINFILE were encountered during 2014 mapping. The extent and importance of these occurrences has yet to be determined, but they are indicative of the mineral potential still to be uncovered in the southern Nicola arc.

### Acknowledgments

We are indebted to past workers in the southern Nicola arc, especially J.W.H. Monger and V.A. Preto, both of whom have generously shared their time and knowledge with us in the field. Discussions and property and drill core visits with Siwash geologists, Brad Benoit and Oliver Saunders, and Tyler Ruks of Kaizen Discovery Inc. greatly aided our understanding of the Siwash gold deposit and the Par prospect.

### References cited

- Armstrong, R. L., and Peto, P., 1981. Eocene quartz-feldspar porphyry intrusions west of Okanagan Lake, southern B.C.: K-Ar dates and Sr isotopic composition. *Northwest Geology*, 10, 13-19.
- Banks, P.C., 1980. Geological and geochemical surveys on the Siwash Creek copper property. In: British Columbia Ministry of Energy, Mines, and Petroleum Resources, Assessment Report 7,987.
- Beatty, T.W., Orchard, M.J., Mustard, P.S., 2006. Geology and tectonic history of the Quesnel Terrane in the area of Kamloops, British Columbia. In: Colpron, M. and Nelson, J.L., (Eds.), *Paleozoic Evolution and Metallogeny of Pericratonic Terranes at the Ancient Pacific Margin of North America*, Canadian and Alaskan Cordillera: Geological Association of Canada, Special Paper 45, pp. 483-504.
- Belasky, P., Stevens, C.H., and Hanger, R.A., 2002. Early Permian location of western North American terranes based on brachiopod, fusulinid, and coral biogeography. *Palaeogeography, Palaeoclimatology and Palaeoecology*, 179, 245-266.
- Bergey, W.R., 1999. Report on geological survey, PAR claims. In: BC Ministry of Energy, Mines, and Petroleum Resources, Assessment Report #25,965.
- Bordet, E., Mihalynuk, M.G., Hart, C.J.R., Mortensen, J.K., Friedman, R.M., and Gabites, J., 2013. Chronostratigraphy of Eocene volcanism, central British Columbia. *Canadian Journal of Earth Sciences*, 51, 56-103. doi:10.1139/cjes-2013-0073
- Breitsprecher, K., Mortensen, J.K., 2004. BCAGE 2004A-1: A database of isotopic age determinations for rock units from British Columbia. British Columbia Ministry of Energy and Mines, British Columbia Geological Survey Open, Open File 2004-3.
- Briskely, J.A., 2005. Indium in zinc-lead and other mineral deposits: a reconnaissance survey of 1118 Indium analyses published before 1985. United States Geological Survey, Open-File Report 2005-1209, 8p.
- Brown, R., and Journeay, J., 1987. Tectonic denudation of the Shuswap metamorphic terrane of southeastern British Columbia. *Geology*, 15, 142-146. doi:10.1130/0091-7613(1987)15<142:TDO TSM>2.0.CO;2
- Campbell, R.B., 1966. Tectonics of the south central cordillera of British Columbia. In: *Tectonic History and Mineral Deposits of the Western Cordillera*. Canadian Institute of Mining, Special Volume, 8, pp. 61-72.
- Christopher, P.A., 1973. Preliminary geological map of the Aspen Grove area, British Columbia, BC Ministry of Energy Mines and Petroleum Resources, British Columbia Geological Survey Preliminary Map No. 10.
- Cohen, K.M., Finney, S.C., Gibbard, P.L., and Fan, J.X., 2013. The ICS international chronostratigraphic chart. *Episodes*, 36, 199-204.
- Crowley, J.L., Schoene, B. and Bowering, S.A., 2007. U-Pb dating of zircon in the Bishop Tuff at the millennial scale. *Geology*, 35,, 1123-1126.
- Diakow, L.J. and Barrios, A., 2008. Geology, Spences Bridge Group southwest of Merritt, British Columbia (parts of NTS 092H/14, 15 and 092I/2,3); BC Ministry of Energy Mines and Petroleum Resources, British Columbia Geological Survey Open File 2008-8, 1:50 000 scale.
- Diakow, L.J. and Barrios, A., 2009. Geology and mineral occurrences of the mid-Cretaceous Spences Bridge Group near Merritt, southern British Columbia (parts of NTS 092H/14, 15; 092I/2, 3). In: *Geological Fieldwork 2008*, British Columbia Ministry of Energy Mines and Petroleum Resources, British Columbia Geological Survey Paper 2009-1, pp. 63-79.
- Enkin, R.J., 2006. Paleomagnetism and the case for Baja British Columbia. In: Haggart, J.W., Enkin, R.J., and Monger, J.W.H. (Eds.), *Paleogeography of the North American Cordillera: Evidence For and Against Large-Scale Displacements*. Geological Association of Canada, Special Paper 46, 233-253.
- Evenchick, C.A., Poulton, T.P. and McNicoll, V.J., 2010. Nature and significance of the diachronous contact between the Hazelton and Bowser Lake groups (Jurassic), north-central British Columbia. *Bulletin of Canadian Petroleum Geology*, 58, 235-267.
- Ferri, F., 1997. Nina Creek Group and Lay Range Assemblage, north-central British Columbia: remnants of late Paleozoic oceanic and arc terranes. *Canadian Journal of Earth Sciences*, 34, 854-874. doi:10.1139/e17-070
- Fjordland Exploration Inc., 2014. Fjordland and Sumac Drill 153 Metres Grading 0.20% Copper and 0.09 g/t Gold on Dillard Property, Southern British Columbia, press release, November, 18, 2014, <http://www.fjordlandex.com/news/nr14-13.pdf>.
- Gerstenberger, H., and Haase, G., 1997. A highly effective emitter substance for mass spectrometric Pb isotopic ratio determinations. *Chemical Geology*, 136, 309-312.
- Gold Mountain Mining Corporation, 2014. Gold Mountain bulk sample lot 2 gold grade at 22.8 gpt: Gold Mountain Mining Corporation, press release, November 17, 2014, [http://www.aumtn.com/cms/wpcontent/uploads/2014/11/2014\\_11\\_17\\_Gold\\_Mountain\\_Press\\_Release\\_Bulk\\_Sample\\_Lot\\_2\\_Gold\\_Grade\\_22\\_gpt.pdf](http://www.aumtn.com/cms/wpcontent/uploads/2014/11/2014_11_17_Gold_Mountain_Press_Release_Bulk_Sample_Lot_2_Gold_Grade_22_gpt.pdf).
- Gourlay, A.W. 1991. Zig property reverse circulation percussion drilling. In: BC Ministry of Energy, Mines, and Petroleum Resources, Assessment Report #21,406.
- Grove, E.W., 1989. Geological report & work proposal on the Siwash creek property. In: British Columbia Ministry of Energy, Mines, and Petroleum Resources, Assessment Report, 19.
- Harms, T.A., 1986. Structural and tectonic analysis of the Sylvester allochthon, northern British Columbia; implications for paleogeography and accretion. Ph.D. Thesis, University of

- Arizona.
- Henderson, M.A., Mihalynuk, M.G., Creaser, R.A., and Logan, J.M., 2015. Microthermometry and Re-Os age of Cu-Ag mineralization at the Zig prospect, southern Quesnel Terrane. In: Geological Fieldwork 2014, British Columbia Ministry of Energy, Mines and Natural Gas, British Columbia Geological Survey Paper 2015-1, (this volume).
- Hunt, P.A., and Roddick, J.C., 1990. A compilation of K–Ar ages: report 19. In: Radiogenic Age and Isotopic Studies, Report 3. Geological Survey of Canada, Paper 89-02, 153-190.
- Ickert, R.B., Thorkelson, D.J., Marshall, D.D., and Ullrich, T.D., 2009. Eocene adakitic volcanism in southern British Columbia: remelting of arc basalt above a slab window. *Tectonophysics*, 464, 164-185.
- Jaffey, A.H., Flynn, K.F., Glendenin, L.E., Bentley, W.C., and Essling, A.M., 1971. Precision measurement of half-lives and specific activities of <sup>235</sup>U and <sup>238</sup>U. *Physics Review*, C4, 1889-1906.
- Kaizen Discovery Inc., 2014. Kaizen Discovery announces positive results of phase-one drilling at Aspen Grove Copper Project in British Columbia, Canada: multiple potential targets established for 2015 phase-two drilling. Kaizen Discovery Inc. press release, December, 10, 2014. [http://www.kaizendiscovery.com/s/news\\_releases.asp?ReportID=687190&\\_Type=News-Releases&Title=Kaizen-Discovery-announces-positive-results-of-phase-one-drillingbrat-Aspen](http://www.kaizendiscovery.com/s/news_releases.asp?ReportID=687190&_Type=News-Releases&Title=Kaizen-Discovery-announces-positive-results-of-phase-one-drillingbrat-Aspen)
- Kwong, Y.T.J., 1987. Evolution of the Iron Mask batholith and its associated copper mineralization: British Columbia Ministry of Energy, Mines and Petroleum Resources, British Columbia Geological Survey, Bulletin 77, 55p.
- Lefebvre, D.V., 1976. Geology of the Nicola Group in the Fairweather Hills, B.C., M.Sc. Thesis, Queen's University, 179p.
- Liu, L., Gurnis, M., Seton, M., Saleeby, J., Müller, R.D., and Jackson, J.M., 2010. The role of oceanic plateau subduction in the Laramide orogeny. *Nature Geoscience*, 3, 353-357.
- Livaccari, R.F., Burke, K., and Sengor, A.M.C., 1981. Was the Laramide orogeny related to subduction of an oceanic plateau? *Nature*, 289, 276-278.
- Logan, J.M. and Mihalynuk, M.G., 2005a. Regional geology and setting of the Cariboo, Bell, Springer and Northeast porphyry Cu-Au zones at Mount Polley, south-central British Columbia. In: Geological Fieldwork 2004, British Columbia Ministry of Energy and Mines, British Columbia Geological Survey Paper 2005-1, 249-270.
- Logan, J.M., and Mihalynuk, M.G., 2005b. Porphyry Cu-Au deposits of the Iron Mask batholith, southeastern BC. In: Geological Fieldwork 2004, British Columbia Ministry of Energy and Mines, British Columbia Geological Survey Paper 2005-1, 271-290.
- Logan, J.M., and Mihalynuk, M.G., 2014. Tectonic controls on early Mesozoic paired alkaline porphyry deposit belts (Cu-Au-Ag-Pt-Pd-Mo) within the Canadian Cordillera. *Economic Geology*, 109, 827-858.
- Ludwig, K.R., 2003. Isoplot 3.09: a geochronological toolkit for Microsoft Excel. Berkeley Geochronology Center, Special Publication 4, Berkeley.
- Massey, N.W.D., MacIntyre, D.G., Desjardins, P.J., and Cooney, R.T., 2005. Digital Geology Map of British Columbia: Whole Province. British Columbia Ministry of Energy, Mines, and Natural Gas, British Columbia Geological Survey, GeoFile 2005-1.
- Massey, N.W.D., and Dostal, J., 2013. Geochemistry of metabasalts from the Knob Hill complex and Anarchist Group in the Paleozoic basement to southern Quesnellia. British Columbia Ministry of Energy, Mines, and Natural Gas, British Columbia Geological Survey, GeoFile 2013-1.
- Mathews, W.H., 1989. Neogene Chilcotin basalts in south-central British Columbia: geology, ages, and geomorphic history. *Canadian Journal of Earth Sciences*, 26, 969-982. doi:10.1139/e89-078
- Mattinson, J.M., 2005. Zircon U-Pb chemical abrasion (CA-TIMS) method: combined annealing and multi-step partial dissolution analysis for improved precision and accuracy of zircon ages. *Chemical Geology*, 220, 47-66.
- McCaffrey, R., Zwick, P.C., Bock, Y., Prawirodirdjo, L., Genrich, J.F., Stevens, C.W., Puntodewo, S.S.O. and Subarya, C., 2000. Strain partitioning during oblique plate convergence in northern Sumatra: geodetic and seismologic constraints and numerical modeling. *Journal of Geophysical Research*, 105, 28,363-28,376.
- Mihalynuk, M.G., Nelson, J. and Diakow, L., 1994. Cache Creek terrane entrapment: oroclinal paradox within the Canadian Cordillera. *Tectonics*, 13, 575-595.
- Mihalynuk, M.G., Erdmer, P., Ghent, E.D., Archibald, D.A., Friedman, R.M., Cordey, F., Johannson, G.G., and Beanish, J., 1999. Age constraints for emplacement of the northern Cache Creek terrane and implications of blueschist metamorphism. In: Geological Fieldwork 1998, British Columbia Ministry of Energy, Mines and Petroleum Resources, British Columbia Geological Survey Paper 1999-1, 127-141.
- Mihalynuk, M., Erdmer, P., Ghent, E.D., Cordey, F., Archibald, D.A., Friedman, R.M., and Johannson, G.G., 2004. Coherent French Range blueschist: subduction to exhumation in <2.5 m.y.? *Geological Society of America Bulletin*, 116, 910-922.
- Mihalynuk, M.G., Logan, J., Friedman, R.M., and Preto, V.A., 2010. Age of mineralization and 'mine dykes' at Copper Mountain alkaline copper-gold-silver porphyry deposit (NTS 092H/07), south-central British Columbia. In: Geological Fieldwork 2009, British Columbia Ministry of Energy, Mines and Petroleum Resources, British Columbia Geological Survey Paper 2010-1, 163-172.
- Mihalynuk, M.G., Logan, J.M., 2013a. Geological setting of Late Triassic Cu-Au porphyry mineralization at Miner Mountain, Princeton. In: Geological Fieldwork 2012, British Columbia Ministry of Energy, Mines and Natural Gas, British Columbia Geological Survey Paper 2013-1, 81-96.
- Mihalynuk, M.G., Logan, J.M., 2013b. Geological setting of Late Triassic Cu-Au porphyry mineralization at the Dillard-Primer prospects near Merritt. In: Geological Fieldwork 2012, British Columbia Ministry of Energy, Mines and Natural Gas, British Columbia Geological Survey Paper 2013-1, 97-114.
- Mihalynuk, M.G., Logan, J.M., Diakow, L.J., Friedman, R.M., and Gabites, J., 2014a. Southern Nicola Arc Project (SNAP): preliminary results. In: Geological Fieldwork 2013, British Columbia Ministry of Energy and Mines, British Columbia Geological Survey, Paper 2014-1, 29-57.
- Mihalynuk, M.G., Friedman, R.M., Gabites, J.E., Logan, J.M., 2014b. Southern Nicola Arc Project 2013: Geochronological data. British Columbia Ministry of Energy and Mines, British Columbia Geological Survey, GeoFile 2014-3.
- Mihalynuk, M.G., Friedman, R.M. and Logan, J.M., 2015. Southern Nicola Arc Project 2014: geochronological data. British Columbia Ministry of Energy and Mines, British Columbia Geological Survey, GeoFile 2015-2.
- Monger, J.W.H., 1989. Geology, Hope, British Columbia. Geological Survey of Canada, Map 41-1989, sheet 1, scale 1:250 000.
- Monger, J.W.H. and McMillan, W.J., 1989. Geology, Ashcroft, British Columbia (92I). Geological Survey of Canada, Map 42-1989, sheet 1, scale 1:250 000.
- Monger, J.W.H., and Ross, C.A., 1971. Distribution of fusulinaceans in western Canadian Cordillera. *Canadian Journal of Earth Sciences*, 8, 259-278.
- Monger, J.W.H., Price, R.A., and Tempelman-Kluit, D.J., 1982. Tectonic accretion and the origin of the two major metamorphic and plutonic belts in the Canadian Cordillera. *Geology*, 10, 70–75.
- Mundil, R., Ludwig, K.R., Metcalfe, I., and Renne, P.R., 2004. Age and timing of the Permian mass extinctions: U/Pb dating of closed-

- system zircons. *Science*, 305, 1760-1763.
- Nance, R.D., Gutiérrez-Alonso, G., Keppie, J.D., Linnemann, U., Murphy, J.B., Quesada, C., Strachan, R.A., and Woodcock, N.H., 2012. A brief history of the Rheic ocean. *Geoscience Frontiers*, 3, 125–135.
- Nelson, W. and Walker, J.T., 1972. Combined Geological and Geophysical Report on the Adonis Property. In: BC Ministry of Energy, Mines, and Petroleum Resources, Assessment Report #04495.
- Nixon, G.T., Archibald, D.A., Heaman, L.M., 1993.  $^{40}\text{Ar}$ - $^{39}\text{Ar}$  and U-Pb geochronometry of the Polar is alaskan-type complex, British Columbia: precise timing of Quesnellia-North America interaction. In: Geological Association of Canada, Mineralogical Association of Canada, Annual Meeting, Program with Abstracts, Waterloo, ON, Canada, pp. A76.
- Parrish, R.R., Monger, J.W.H., 1992. New U-Pb dates from southwestern British Columbia. Geological Survey of Canada, Paper 91-2, Radiogenic Age Isotopic Studies Report, 5, 87-108.
- Patton, C., Hellstrom, J., Paul, B., Woodhead, J., and Hergt, J., 2011. Iolite: freeware for the visualization and processing of mass spectrometry data. *Journal of Analytical Atomic Spectroscopy*, 26, 2508-2518.
- Pooley, R., Lomas, S., Hawthorn, G., and Alexander, R.B., 2011. NI 43-101 technical report for a preliminary economic assessment on the Elk Gold Project, Merritt, British Columbia, Canada: prepared for Almaden Minerals and Beanstalk Capital Inc., 141p.
- Preto, V.A., 1979. Geology of the Nicola Group between Merritt and Princeton: British Columbia Ministry of Energy, Mines and Petroleum Resources, British Columbia Geological Survey, Bulletin 69, 90p.
- Ray, G.E., and Dawson, G.L., 1994. The geology and mineral deposits of the Hedley gold skarn district, southern British Columbia. British Columbia Ministry of Energy, Mines and Petroleum Resources, Bulletin 87, 156p.
- Ray, G.E., Webster, I.C.L., Dawson, G.L., and Ettliger, A.D., 1993. A geological overview of the Hedley gold skarn district, southern British Columbia (92H). In: Geological Fieldwork 1992, British Columbia Ministry of Energy, Mines and Petroleum Resources, British Columbia Geological Survey Paper 1994-1, 269-279.
- Read, P.B., and Okulitch, A.V., 1977. The Triassic unconformity of south-central British Columbia. *Canadian Journal of Earth Sciences*, 14, 606-638.
- Rice, H.M.A., 1947. Geology and mineral deposits of the Princeton map area, British Columbia. Geological Survey of Canada, Memoir 243, 136p.
- Ricketts, B.D., Evenchick, C.A., Anderson, R.G., and Murphy, D.C., 1992. Bowser Basin, northern British Columbia: constraints on the timing of initial subsidence and Stikinia-North America terrane interactions. *Geology*, 20, 1119-1122.
- Ross, C.A., and Ross, J.R.P., 1983. Late Paleozoic accreted terranes of western North America. In: Stevens, C.H. (Ed.), *Pre-Jurassic Rocks in Western North American Suspect Terranes*. Society of Economic Paleontologists and Mineralogists, 7-22.
- Ross, C.A., and J.R.P. Ross., 1985. Carboniferous and Early Permian biogeography. *Geology*, 13, 27-30.
- Schau, M.P., 1968. Geology of the Upper Triassic Nicola Group in south central British Columbia. Ph.D. Thesis, The University of British Columbia, Vancouver, Canada, 211 p.
- Schmitz, M.D., and Schoene, B., 2007. Derivation of isotope ratios, errors, and error correlations for U-Pb geochronology using  $^{205}\text{Pb}$ - $^{235}\text{U}$ -( $^{233}\text{U}$ )-spiked isotope dilution thermal ionization mass spectrometric data. *Geochemistry, Geophysics, Geosystems*, 8, Q08006. doi:10.1029/2006GC001492
- Scoates, J.S. and Friedman, R.M., 2008. Precise age of the platiniferous Merensky Reef, Bushveld Complex, South Africa, by the U-Pb ID-TIMS chemical abrasion ID-TIMS technique, *Economic Geology*, 103, 465-471.
- Sigloch, K., Mihalynuk, M.G., 2013. Intra-oceanic subduction shaped the assembly of Cordilleran North America. *Nature*, 496, 50-56.
- Sláma, J., Košler, J., Condon, D.J., Crowley, J.L., Gerdes, A., Hanchar, J.M., Horstwood, M.S.A., Morris, G.A., Nasdala, L., Norberg, N., Schaltegger, U., Xchoene, B., Tubrett, M.N., and Whitehouse, M.J., 2007. Plešovice zircon - A new natural reference material for U-Pb and Hf isotopic microanalysis. *Chemical Geology*, 249, 1-35.
- Sluggett, C.L., 2008. Quaternary alkaline and calc-alkaline basalts in southern British Columbia: mixed signals from mantle sources above the southern edge of the Juan de Fuca-Pacific slab window. M.Sc. thesis, Simon Fraser University, Vancouver, Canada, 153p.
- Struik, L.C., Orchard, M.J., 1985. Late Paleozoic conodonts from ribbon chert delineate imbricate thrusts within the Antler Formation of the Slide Mountain terrane, central British Columbia. *Geology*, 13, 794-798.
- Tafti, R., Mortensen, J.K., Lang, J.R., Rebagliati, M., and Oliver, J.L., 2009. Jurassic U-Pb and Re-Os ages for newly discovered Xietongmen Cu-Au porphyry district, Tibet: implications for metallogenic epochs in the southern Gangdese Belt. *Economic Geology*, 104, 127–136.
- Thirlwall, M.F., 2000. Inter-laboratory and other errors in Pb isotope analyses investigated using a  $^{207}\text{Pb}$ - $^{204}\text{Pb}$  double spike, *Chemical Geology*, 163, 299-322.
- Thompson, R.I., Glombick, P., Erdmer, P., Heaman, L.M., Lemieux, Y., and Daughtry, K.L., 2006. Evolution of the ancestral Pacific margin, southern Canadian Cordillera: insights from new geologic maps. In: Colpron, M., and Nelson, J.L. (Eds.), *Paleozoic Evolution and Metallogeny of Pericratonic Terranes at the Ancient Pacific Margin of North America*, Canadian and Alaskan Cordillera. Geological Association of Canada, Special Paper 45, 433-482.
- Thorkelson, D.J., and Rouse, G.E., 1989. Revised stratigraphic nomenclature and age determinations for mid-Cretaceous volcanic rocks in southwestern British Columbia. *Canadian Journal of Earth Sciences*, 26, 2016-2031.